Ground-state energies, densities and momentum distributions in closed-shell nuclei calculated within a cluster expansion approach and realistic interactions

M. Alvioli,[1] C. Ciofi degli Atti,[1] and H. Morita[2]
[1]*Department of Physics, University of Perugia and Istituto Nazionale di Fisica Nucleare, Sezione di Perugia, Via A. Pascoli, I-06123, Perugia, Italy*
[2]*Sapporo Gakuin University, Bunkyo-dai 11, Ebetsu 069-8555, Hokkaido, Japan*
(Received 4 July 2005; published 16 November 2005)

A linked cluster expansion suitable for the treatment of ground-state properties of complex nuclei, as well as of various particle-nucleus scattering processes, has been used to calculate the ground-state energy, density, and momentum distribution of ^{16}O and ^{40}Ca in terms of realistic interactions. First, a benchmark calculation for the ground-state energy is performed with the truncated $V8'$ potential and consisting of the comparison of our results with the ones obtained by the Fermi hypernetted chain approach, adopting in both cases the same mean-field wave functions and the same correlation functions. The results exhibited a nice agreement between the two methods. Therefore the approach has been applied to the calculation of the ground-state energy, density, and momentum distributions of ^{16}O and ^{40}Ca by use of the full $V8'$ potential, and again a satisfactory agreement was found with the results based on more advanced approaches in which higher-order cluster contributions are taken into account. It appears therefore that the cluster expansion approach can provide accurate approximations for various diagonal and nondiagonal density matrices, so that it could be used for a reliable evaluation of nuclear effects in various medium- and high-energy scattering processes off nuclear targets. The developed approach can be readily generalized to the treatment of Glauber-type final-state interaction effects in inclusive, semi-inclusive, and exclusive processes off nuclei at medium and high energies.

DOI: 10.1103/PhysRevC.72.054310 PACS number(s): 21.60.−n, 21.10.Dr, 27.20.+n, 27.40.+z

I. INTRODUCTION

Knowledge of the nuclear wave function, in particular its most interesting and unknown part, viz. the correlated one, which is predicted by realistic many-body calculations to strongly deviate from a mean-field description, is not only a prerequisite for understanding the details of bound hadronic systems, but is becoming at present a necessary condition for a correct description of medium- and high-energy scattering processes off nuclear targets; these, in fact, represent nowadays an efficient tool for the investigation of several high-energy problems, e.g., color transparency, hadronization, the properties of dense hadronic matter, etc., that manifest themselves in only the nuclear medium. The necessity of an accurate treatment of the effects of the medium in high-energy scattering processes is becoming a relevant issue in hadronic physics. The problem is not trivial, for one must first solve the many-body problem and then find a way to describe scattering processes in terms of realistic many-body wave functions. The difficulty mainly arises because, even if a reliable and manageable many-body description of the ground state is developed, the problem remains of the calculation of the final state. In the case of *few-body systems*, a consistent treatment of initial-state correlations (ISCs) and final-state interaction (FSI) is nowadays possible at low energies by the solution of the Schrödinger equation for the bound and continuum states (see, e.g. [1–3] and references therein), but at high energies, when the number of partial waves sharply increases and nucleon excitations can occur, the Schrödinger approach becomes impractical and other methods have to be employed. Moreover, in the case of *complex nuclei*, additional difficulties arise because of the approximations that are still necessary for solving the many-body problem. As a matter of fact, in spite of the relevant progress made in recent years in the calculation of the properties of light nuclei (see, e.g. [4–8]), much remains to be done, also in view that the results of very sophisticated calculations (e.g., the variational Monte Carlo ones [5]) show that the wave function that minimizes the expectation value of the Hamiltonian provides a very poor nuclear density; moreover, the structure of the best trial wave function is so complicated that its use in the calculation of various processes at intermediate and high energies appears to be no easy task. It is for this reason that the evaluation of nuclear effects in medium- and high-energy scattering processes is usually carried out within simplified models of nuclear structure. As a matter of fact, ISCs are often introduced by a procedure that has little to recommend itself, namely the expectation value of the transition operator is evaluated with shell-model (SM) uncorrelated wave functions and the initial two-body wave function describing the independent relative motion of two nucleons is replaced with a phenomenological-correlated wave function. Recently, however, important progress has been made in that ISCs have been introduced from the beginning by use of correlated wave functions and cluster expansion techniques. Central Jastrow-type correlations have been often used to investigate the effects of ISCs on various scattering processes off complex nuclei induced by medium-energy leptons like $A(e,e')X$ [9], $A(e,e'p)X$ [10], and $A(e,e'2N)X$ [11] processes. Calculations of inclusive electron scattering have also been performed with realistic many-body wave functions and spectral functions within various approximations [12,13], and noncentral correlations have been recently introduced in the calculations of $A(e,e'p)B$ and $A(e,e'2N)B$ [14,15]. In spite of this progress, further work remains to be done to

achieve a full consistent treatment of both the ISC and FSI in intermediate- and high-energy scattering off complex nuclei. This would be particularly urgent as far as various high-energy scattering phenomena are concerned, e.g., exclusive processes at high-momentum transfer [16], inclusive [17] and semi-inclusive [18] hadron production in deep inelastic scattering, and others, that might also require a careful treatment of nuclear effects. As a matter of fact, a recent calculation [19] of the integrated nuclear transparency in the processes $^{16}\mathrm{O}(e,e'p)X$ and $^{40}\mathrm{Ca}(e,e'p)X$ performed within a cluster expansion approach, including realistic central and tensor correlations, shows that the results do depend on both the SM and the ISC parameters, which therefore have to be fixed from firm criteria, e.g., from the calculation of the static properties of nuclei, like the ground-state energy and the density distribution.

For such a reason, we have undertaken the calculation of the basic ground-state properties (energies, densities, and momentum distributions) of complex nuclei within a framework, the cluster expansion technique, which can easily be generalized to the treatment of various scattering processes, keeping the basic features of ISCs as predicted by the structure of realistic nucleon-nucleon (*NN*) interactions. Our approach is presented in detail in this paper, which is organized as follows: In Sec. II some basic ideas concerning the application of the cluster expansion techniques to the approximate solution of the nuclear many-body problem are recalled; the cluster expansion used in the calculations is described in Sec. III; the ground-state energy calculations for ^{16}O and ^{40}Ca are presented in Sec. IV, where the results of a benchmark calculation, aimed at a comparison of our results with the results obtained within the fermion hypernetted chain (FHNC) approach [7,8,20], are presented; the results of the calculations of the charge densities and momentum distributions are given in Secs. V and VI, respectively; the diagrammatic representation of the cluster expansion approach are illustrated in Sec. VII; the summary and conclusions are presented in Sec. VIII.

Preliminary results of our calculations have been presented in Refs. [21,22].

II. THE CORRELATED WAVE FUNCTIONS

It is well known that if nuclei are considered to be aggregates of pointlike nucleons with the same properties and interactions as those of the free ones, and, moreover, all degrees of freedom but nucleonic ones are frozen, the nuclear many-body problem reduces to the search of the eigenvalues and eigenfunctions of the following Schrödinger equation [23]:

$$\left[\sum_{i=1}^{A}\frac{\boldsymbol{p}_i^2}{2M_N}+\hat{V}_{\mathrm{eff}}(1,2,\ldots,A)\right]\times\psi_n(1,2,\ldots,A)=E_n\,\psi_n(1,2,\ldots,A),\qquad(1)$$

where M_N is the nucleon mass, and the effective interaction includes many-body interactions between the constituents, i.e.,

$$\hat{V}_{\mathrm{eff}}(1,2,\ldots,A)=\sum_{i<j}\hat{v}_2(i,j)+\sum_{i<j<k}\hat{v}_3(i,j,k)+\cdots+v_A(1,2,\ldots,A).\qquad(2)$$

Within the so-called *standard model* of nuclei [24], which is considered from now on, many-body interactions are disregarded and we solve Eq. (1), keeping only the two-body interaction $\hat{v}_2(i,j)$, whose form is determined from two-body bound and scattering data. We consider therefore the following nuclear Hamiltonian:

$$\hat{H}=\hat{T}+\hat{V}=-\frac{\hbar^2}{2M_N}\sum_{i=1}^{A}\nabla_i^2+\sum_{i<j}\hat{v}_2(\boldsymbol{x}_i,\boldsymbol{x}_j),\qquad(3)$$

where the vector $\boldsymbol{x}$ denotes the set of nucleonic degrees of freedom, i.e., $\boldsymbol{x}\equiv(\boldsymbol{r};\boldsymbol{\sigma};\boldsymbol{\tau})$, with $\boldsymbol{r},\boldsymbol{\sigma}$, and $\boldsymbol{\tau}$ denoting the spatial, spin, and isospin coordinates, respectively. We try to find the solution of the Schrödinger equation pertaining to the ground state of the nucleus, i.e.,

$$\hat{H}\,\psi_o=E_o\,\psi_o,\qquad(4)$$

and to this end we look for the ground-state wave function ψ_0 that minimizes the expectation value of the Hamiltonian:

$$\langle\hat{H}\rangle=\frac{\langle\psi_o|\hat{H}|\psi_o\rangle}{\langle\psi_o\,|\,\psi_o\rangle}\geqslant E_o.\qquad(5)$$

As a trial wave function we use a correlated wave function of the following form [25]:

$$\psi_o(\boldsymbol{x}_1,\ldots,\boldsymbol{x}_A)=\hat{F}(\boldsymbol{x}_1,\ldots,\boldsymbol{x}_A)\,\phi_o(\boldsymbol{x}_1,\ldots,\boldsymbol{x}_A),\qquad(6)$$

where ϕ_o is a SM mean-field wave function describing the independent particle motion and $\hat{F}$ is a symmetrized *correlation operator*, which generates correlations into the mean-field wave function; the correct symmetry of the wave function is guaranteed by ϕ_o.

As in any variational approach, the central problem here is to give an explicit form to the trial wave function [Eq. (6)]; whereas for ϕ_o any realistic SM wave function can be considered a physically sound approximation, the choice of the form of the operator $\hat{F}$ is not clear *a priori*. However, one can be guided by the knowledge of the basic features of the force acting between the considered hadrons. Nowadays the nucleon-nucleon interaction can be cast in the following form [26]:

$$\hat{V}=\sum_{n=1}^{N}v^{(n)}(r_{ij})\,\hat{\mathcal{O}}_{ij}^{(n)},\qquad(7)$$

where $r_{ij}=|\boldsymbol{r}_i-\boldsymbol{r}_j|$ is the relative distance of nucleons i and j, and n, ranging up to $N=18$, labels the state-dependent operator $\hat{\mathcal{O}}_{ij}^{(n)}$. In this paper we limit ourselves to $N=6$, in which case we have

$$\begin{aligned}
&\hat{\mathcal{O}}_{ij}^{(1)}\equiv\hat{\mathcal{O}}_{ij}^{c}=1, && \hat{\mathcal{O}}_{ij}^{(2)}\equiv\hat{\mathcal{O}}_{ij}^{\sigma}=\boldsymbol{\sigma}_i\cdot\boldsymbol{\sigma}_j,\\
&\hat{\mathcal{O}}_{ij}^{(3)}\equiv\hat{\mathcal{O}}_{ij}^{\tau}=\boldsymbol{\tau}_i\cdot\boldsymbol{\tau}_j, && \hat{\mathcal{O}}_{ij}^{(4)}\equiv\hat{\mathcal{O}}_{ij}^{\sigma\tau}=(\boldsymbol{\sigma}_i\cdot\boldsymbol{\sigma}_j)(\boldsymbol{\tau}_i\cdot\boldsymbol{\tau}_j),\\
&\hat{\mathcal{O}}_{ij}^{(5)}\equiv\hat{\mathcal{O}}_{ij}^{t}=\hat{S}_{ij}, && \hat{\mathcal{O}}_{ij}^{(6)}\equiv\hat{\mathcal{O}}_{ij}^{t\tau}=\hat{S}_{ij}(\boldsymbol{\tau}_i\cdot\boldsymbol{\tau}_j).
\end{aligned}\qquad(8)$$

Accordingly, the operator $\hat{F}$ is written as

$$\hat{F}(\boldsymbol{x}_1, \boldsymbol{x}_2 \cdots \boldsymbol{x}_A) = \hat{S} \prod_{i<j}^{A} \hat{f}(r_{ij}), \tag{9}$$

with

$$\hat{f}(r_{ij}) = \sum_{n=1}^{N} \hat{f}^{(n)}(r_{ij}), \qquad \hat{f}^{(n)}(r_{ij}) = f^{(n)}(r_{ij})\, \hat{O}_{ij}^{(n)}. \tag{10}$$

The variational principle requires the full evaluation of Eq. (5), which, obviously, is no easy task because of the structure of ψ_0. We evaluate the expectation value of Hamiltonian (5) by using the cluster expansion techniques [25], adopting a specific cluster expansion that is described in the next section.

III. THE CLUSTER EXPANSION

The evaluation of the expectation value of $\hat{H}$ is an object of intensive activity, which in the past few years has produced considerable results: The approximate solution of the Schrödinger equation by means of Monte Carlo methods, for example, has reached a great level of accuracy, and the ground-state properties of nuclei with $A = 16$ have been obtained with a full evaluation of Eq. (5) [4,5]; exhaustive calculations have also been performed within the FHNC approximation [7,8,20]. Nevertheless, the level of complexity of these calculations often prevents the wave function from being used with reasonable ease in other nuclear-related problems, such as nuclear reactions. Our goal is to present a more economical, but effective, method for the calculation of the expectation value of any quantum-mechanical operator $\hat{A}$ in the many-body ground-state described by the wave function ψ_o, i.e.,

$$\langle \hat{A} \rangle = \frac{\langle \psi_o | \hat{A} | \psi_o \rangle}{\langle \psi_o \,|\, \psi_o \rangle}, \tag{11}$$

with ψ_o having the structure of Eq. (6). In this section we introduce a cluster expansion technique in order to evaluate Eq. (11). To begin, in this section, a generic operator $\hat{A}$ is considered, whereas in the next section, we consider the Hamiltonian operator and the one-body denesity (OBD) and two-body density (TBD) matrix operators.

Various types of cluster expansions have been used in the past to calculate the ground-state properties of nuclei (see, e.g., [27,28]); in these calculations, mainly aimed at investigating the convergence of the expansion, simple models of the *NN* interaction have been usually used. In this paper we use an expansion that, to our knowledge, has never been used previously to calculate ground-state properties of nuclei in terms of realistic interactions. The expansion we use was originally developed in Ref. [29] (see also [30] and [31]) in the case of central Jastrow-type correlations; the main feature of such an expansion is that it is linked and number conserving. The latter property means that the normalization of any observable is provided by the normalization of the mean-field wave function, i.e., by the first term of the expansion: the contribution of all other terms to the normalization vanishes analytically order by order. The expansion, called the η *expansion,* was originally used to obtain the lowest-order correlation contribution to the diagonal OBD matrix $\rho(\boldsymbol{r}_1)$, to the one-body mixed-density (OBMD) matrix $\rho(\boldsymbol{r}_1, \boldsymbol{r}'_1)$, and to the TBD matrix $\rho_2(\boldsymbol{r}_1, \boldsymbol{r}_2; \boldsymbol{r}'_1, \boldsymbol{r}'_2)$, by use of central correlations only [i.e., Eqs. (9) and (10) with $N = 1$] [29,30]. Subsequently [32], the lowest-order expansion of the OBMD operator has been generalized to take into account also the noncentral spin-isospin and tensor-isospin correlations $f^{(4)}$ and $f^{(6)}$ in Eqs. (10), which turned out to be the most relevant noncentral correlation functions in nuclear matter [33], as well as all correlations up to[1] $N = 6$ [7]. During the past few years, lowest-order expansions have also been applied, within the central correlation approximation, to the calculation of the TBD matrix [34] and of various transition matrix elements appearing in inclusive $A(e, e')X$ and exclusive $A(e, e'p)B$ and $A(e, e'2N)B$ processes (see, e.g., Refs. [9–12]). As already mentioned, the expansion has also been used, within the f_3 approximation, to calculate the nuclear transparency in the semi-inclusive process $A(e, e'p)X$ [19]. To our knowledge, the η expansion has never been used to calculate the ground-state energy of complex nuclei with a realistic interaction. It is precisely the central aim of our work to present a detailed report of the results of the calculation of the ground-state energy, density, and momentum distributions of complex nuclei by using the η expansion and realistic interactions.

Let us outline the basic features of the expansion and, to this end, let us first consider, for ease of presentation, the average value of a spin-isospin-independent operator $\hat{A}$. Let us moreover consider closed-shell nuclei with equal numbers of protons and neutrons, i.e., $N = Z$ (the generalization to the case $N \neq Z$ is straightforward). Following the formal expression for ψ_o in Eq. (6), taking the correlation operator $\hat{F}$ as in Eq. (9), and introducing the quantity

$$\hat{\eta}_{ij} \equiv \hat{f}_{ij}^{\dagger}\, \hat{f}_{ij} - 1, \tag{12}$$

we can write the expectation value (11) as follows:

$$\begin{aligned}
\langle \hat{A} \rangle &= \frac{\langle \phi_o | \hat{F}^{\dagger}\, \hat{A}\, \hat{F}\, | \phi_o \rangle}{\langle \phi_o |\, \hat{F}^{\dagger}\, \hat{F}\, | \phi_o \rangle} \\
&= \langle \phi_o | \prod_{i<j} \left(1 + \hat{\eta}_{ij}\right) \hat{A} | \phi_o \rangle \langle \phi_o | \prod_{i<j} \left(1 + \hat{\eta}_{ij}\right) | \phi_o \rangle^{-1} \\
&= \langle \phi_o | (1 + \sum_{i<j} \hat{\eta}_{ij} + \sum_{(i<j)<(k<l)} \hat{\eta}_{ij} \hat{\eta}_{kl} + \cdots)\, \hat{A}\, | \phi_o \rangle \\
&\quad \times \left[1 + \langle \phi_o | \sum_{i<j} \hat{\eta}_{ij} | \phi_o \rangle + \cdots \right]^{-1}.
\end{aligned} \tag{13}$$

[1] The approximation, that includes only the components $n = \{1, 4, 6\}$ is usually referred to as the f_3 *approximation*, whereas the approximation that includes all correlations up to $N = 6$ is referred to as the f_6 *approximation*.

Expanding in series the denominator ($[1+x]^{-1} = 1 - x + x^2 - \cdots$) one obtains

$$\langle \hat{A} \rangle = \left[\langle \phi_o | \hat{A} | \phi_o \rangle + \langle \phi_o | \sum_{i<j} \hat{\eta}_{ij} \hat{A} | \phi_o \rangle + \cdots \right] \times \left[1 - \langle \phi_o | \sum_{i<j} \hat{\eta}_{ij} | \phi_o \rangle + \langle \phi_o | \sum_{i<j} \hat{\eta}_{ij} | \phi_o \rangle^2 + \cdots \right], \tag{14}$$

and collecting all terms containing the same number of functions $\hat{\eta}_{ij}$, one obtains the infinite series

$$\langle \hat{A} \rangle = \langle \hat{A} \rangle_o + \langle \hat{A} \rangle_1 + \langle \hat{A} \rangle_2 + \cdots + \langle \hat{A} \rangle_n + \cdots. \tag{15}$$

At second order in η, one has, explicitly,

$$\langle \hat{A} \rangle_0 = \langle \phi_o | \hat{A} | \phi_o \rangle, \tag{16a}$$

$$\langle \hat{A} \rangle_1 = \langle \phi_o | \sum_{i<j} \hat{\eta}_{ij} \hat{A} | \phi_o \rangle - \langle \hat{A} \rangle_o \langle \phi_o | \sum_{i<j} \hat{\eta}_{ij} | \phi_o \rangle, \tag{16b}$$

$$\langle \hat{A} \rangle_2 = \langle \phi_o | \sum_{(i<j)<(k<l)} \hat{\eta}_{ij} \hat{\eta}_{kl} \hat{A} | \phi_o \rangle - \langle \phi_o | \times \sum_{i<j} \hat{\eta}_{ij} \hat{A} | \phi_o \rangle \langle \phi_o | \sum_{i<j} \hat{\eta}_{ij} | \phi_o \rangle - \langle \hat{A} \rangle_o \times \left(\langle \phi_o | \sum_{(i<j)<(k<l)} \hat{\eta}_{ij} \hat{\eta}_{kl} | \phi_o \rangle - \langle \phi_o | \sum_{i<j} \hat{\eta}_{ij} | \phi_o \rangle^2 \right) \tag{16c}$$

where the term of the order of n contains $\hat{\eta}_{ij}$ ($\hat{f}_{ij}$) up to the nth ($2n$th) power.

In the general case of spin-isospin-dependent operator $\hat{A}$, as is the case of realistic interaction (7), the formulation of the expansion is of course different because of the noncommutativity of the operators. The preceding equations, however, are still valid provided the product $\hat{\eta}_{ij} \hat{A}$ is replaced with $\hat{f}_{ij} \hat{A} \hat{f}_{ij} - \hat{A}$. The first order of the expansion will then read as follows:

$$\langle \hat{A} \rangle_1 = \langle \phi_o | \sum_{i<j} (\hat{f}_{ij} \hat{A} \hat{f}_{ij} - \hat{A}) | \phi_o \rangle - \langle \hat{A} \rangle_o \langle \phi_o | \sum_{i<j} (\hat{f}_{ij} \hat{f}_{ij} - 1) | \phi_o \rangle, \tag{17}$$

where $\langle \hat{A} \rangle_o$ is given by Eq. (16a). The second-order term can straightforwardly be obtained by the same recipe.

A relevant feature of the η expansion is that the expansion of the denominator ensures that only linked terms contribute to the overall expectation value, all unlinked terms canceling out among themselves. This feature [which obviously holds also for $\langle \hat{A} \rangle_1$ in Eq. (16b)] turns out to be very convenient from a computational point of view, for it reduces the number of terms to be evaluated and allows one to obtain a very systematic and general procedure. It should also be stressed that, because of the noncommutative nature of the operators $\hat{\mathcal{O}}_{ij}$ in Eqs. (10), sets of diagrams involving more than two particles appear in the expectation value of the Hamiltonian already at first order. Eventually we point out that in case of central Jastrow correlations the η_{ij} factor reduces to $\eta_{ij} = f_{ij}^2 - 1$ with $\kappa = \langle \eta_{ij} \rangle$ playing the role of a small expansion parameter [29].

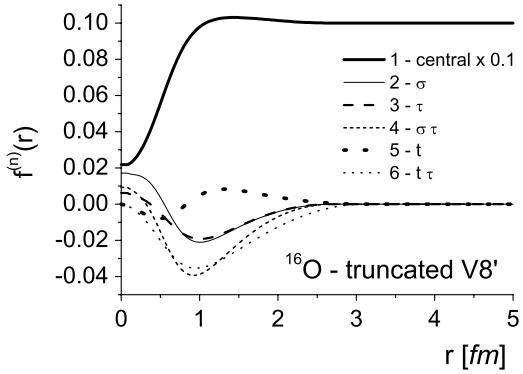

FIG. 1. The correlation functions for ^{16}O corresponding to the truncated Argonne $V8'$ interaction [36] used in the benchmark calculation (after Ref. [9]).

IV. APPLICATION OF THE η EXPANSION TO THE NUCLEI ^{16}O AND ^{40}Ca: GENERAL FORMULAS AND A BENCHMARK CALCULATION WITH TRUNCATED $V8'$ AND $U14$ INTERACTIONS

A. General formulas in terms of density distributions

In what follows the expectation value of the Hamiltonian will always be written in the form

$$E_o = \langle \hat{T} \rangle + \langle \hat{V} \rangle. \tag{18}$$

The average kinetic energy in Eq. (18) is given by

$$\langle \hat{T} \rangle = -\frac{\hbar^2}{2 M_N} \int d\boldsymbol{r}_1 [\nabla_1 \cdot \nabla_{1'} \rho(\boldsymbol{r}_1, \boldsymbol{r}'_1)]_{\boldsymbol{r}_1 = \boldsymbol{r}'_1}, \tag{19}$$

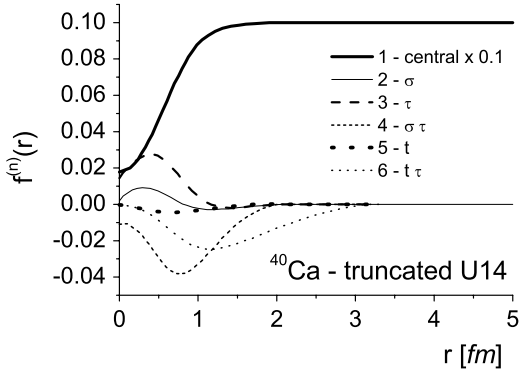

FIG. 2. The correlation functions for ^{40}Ca corresponding to the truncated Urbana $U14$ interaction [38] used in the benchmark calculation (after Ref. [9]).

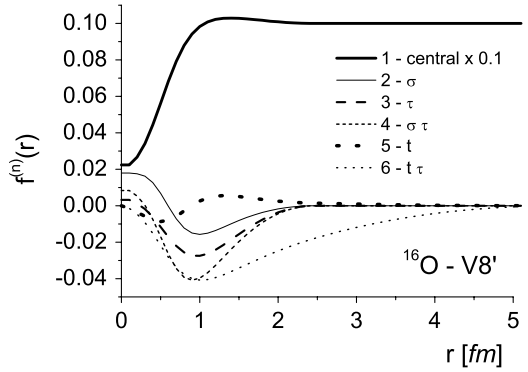

FIG. 3. The correlation functions for ^{16}O corresponding to the full Argonne $V8'$ interaction (after Ref. [7]).

where $\rho(\boldsymbol{r}_1, \boldsymbol{r}'_1)$ is the OBMD matrix defined as the expectation value of the operator

$$\hat{\rho}_1(\tilde{\boldsymbol{r}}_1, \tilde{\boldsymbol{r}}'_1) = \sum_i \delta(\boldsymbol{r}_i - \tilde{\boldsymbol{r}}_1)\,\delta(\boldsymbol{r}'_i - \tilde{\boldsymbol{r}}'_1) \prod_{j\neq i} \delta(\boldsymbol{r}_j - \boldsymbol{r}'_j), \tag{20}$$

i.e.,

$$\rho(\boldsymbol{r}_1, \boldsymbol{r}'_1) = \langle \psi_o | \hat{\rho}\, | \psi'_o \rangle, \tag{21}$$

where

$$\psi_o \equiv \psi_o(\boldsymbol{x}_1, \ldots, \boldsymbol{x}_A), \tag{22}$$

$$\psi'_o \equiv \psi_o(\boldsymbol{x}'_1, \ldots, \boldsymbol{x}'_A). \tag{23}$$

Whereas Eq. (19) is valid for any kind of wave function and interaction, being the kinetic-energy operator a spin-isospin-independent operator, the expression for the average potential energy $\langle \hat{V} \rangle$ does depend on the type of two-body interaction. For a purely central interaction $v^c(r_{12})$ we have

$$\langle \hat{V} \rangle = \int d\boldsymbol{r}_1 d\boldsymbol{r}_2\; v^c(r_{12}) \rho_2(\boldsymbol{r}_1, \boldsymbol{r}_2), \tag{24}$$

where $\rho_2(\boldsymbol{r}_1, \boldsymbol{r}_2)$ is the radial, operator-independent, TBD matrix, summed over spin-isospin variables; it is the expectation value of the radial operator

$$\hat{\rho}_2(\tilde{\boldsymbol{r}}_1, \tilde{\boldsymbol{r}}_2) = \sum_{i<j} \delta(\boldsymbol{r}_i - \tilde{\boldsymbol{r}}_1)\,\delta(\boldsymbol{r}_j - \tilde{\boldsymbol{r}}_2) \prod_k \delta(\tilde{\boldsymbol{r}}_k - \tilde{\boldsymbol{r}}'_k), \tag{25}$$

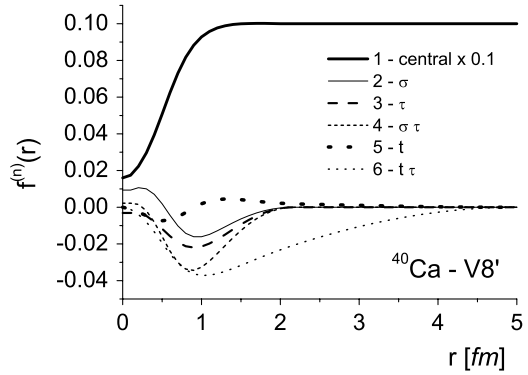

FIG. 4. The correlation functions for ^{40}Ca from [7], corresponding to the $V8'$ interaction [36] (after Ref. [7]).

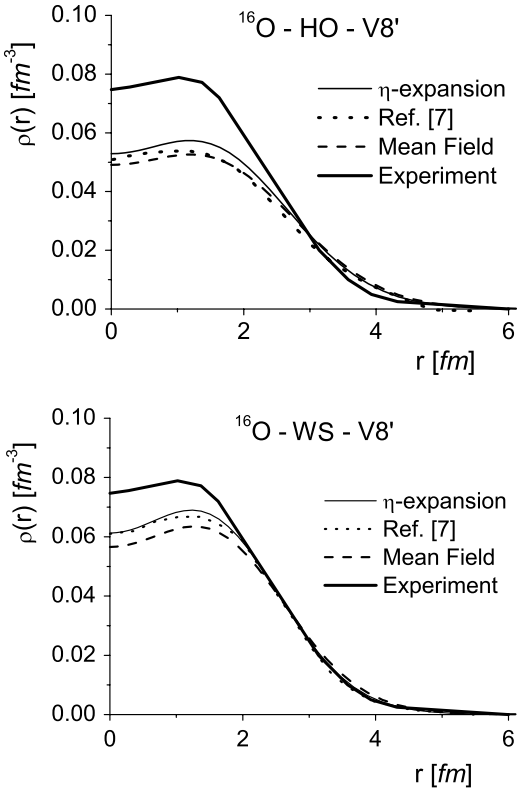

FIG. 5. The charge density of ^{16}O. Thick solid curves, experimental density [42]; thin solid curves, results of the η expansion with harmonic oscillator (HO, top) and Woods-Saxon (WS, bottom) wave functions and correlation functions shown in Fig. 3. The wave-function parameters correspond to the minimization of the ground-state energy. Dotted curves, results from Ref. [7]; dashed curves, mean-field density obtained by setting $f^{(1)} = 1$, $f^{(n\neq 1)} = 0$. The charge density is obtained by folding the matter density with the charge density of the proton and correcting for the center-of-mass motion effects. The value of the rms radius is $\langle r^2 \rangle^{1/2} = 3.07$ fm with HO wave functions and $\langle r^2 \rangle^{1/2} = 2.85$ fm with WS wave functions. The value of the HO parameter is $a = 2.00$ fm and the parameters of the WS well are $V_0 = 42.0$ MeV, $R_0 = 3.6$ fm, and $a_0 = 0.55$ fm. The density normalization is $\int d\boldsymbol{r}\rho(r) = Z$.

i.e.,

$$\begin{aligned}\rho_2(\boldsymbol{r}_1, \boldsymbol{r}_2) &= \langle \psi_o | \hat{\rho}_2 | \psi_o \rangle \\ &= \frac{A(A-1)}{2} \int \prod_{j=3}^{A} d\boldsymbol{r}_j\, |\psi_o(\boldsymbol{r}_1, \boldsymbol{r}_2, \boldsymbol{r}_3, \ldots, \boldsymbol{r}_A)|^2 \\ &\quad \times \left[\int \prod_{j=1}^{A} d\boldsymbol{r}_j\, |\psi_o(\boldsymbol{r}_1, \ldots, \boldsymbol{r}_A)|^2 \right]^{-1}, \end{aligned} \tag{26}$$

where, as in Eq. (21), an implicit summation over the spin and isospin variables is meant to occur (note that from now on the TBD matrix is denoted by subscript 2, i.e., ρ_2, whereas the OBMD matrix is simply denoted by ρ). In the case of an operator-dependent two-body interaction of the type of

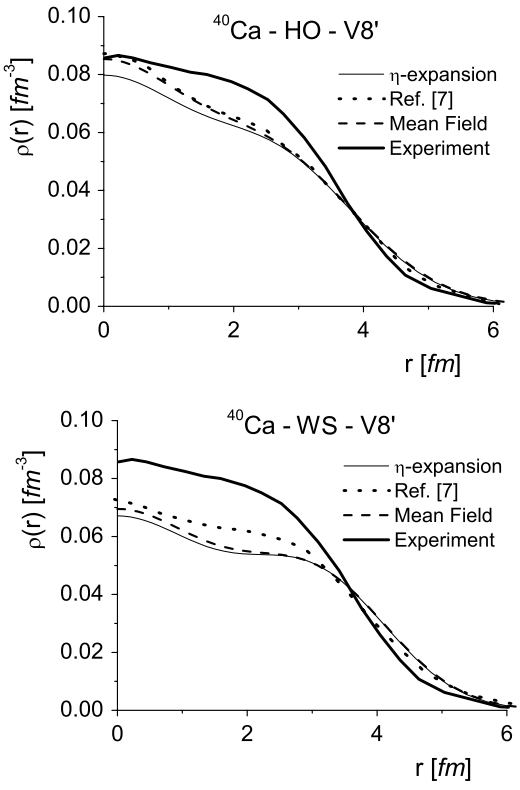

FIG. 6. The same as in Fig. 5, but for ^{40}Ca and correlation functions from Fig. 4. The value of the rms radius is $\langle r^2\rangle^{1/2} = 3.72$ fm, with HO wave functions and $\langle r^2\rangle^{1/2} = 3.75$ fm with WS wave functions; the value of the HO parameter is $a = 2.10$ fm, and the parameters of the WS well are $V_0 = 50.0$ MeV, $R_0 = 5.3$ fm, and $a_0 = 0.53$ fm.

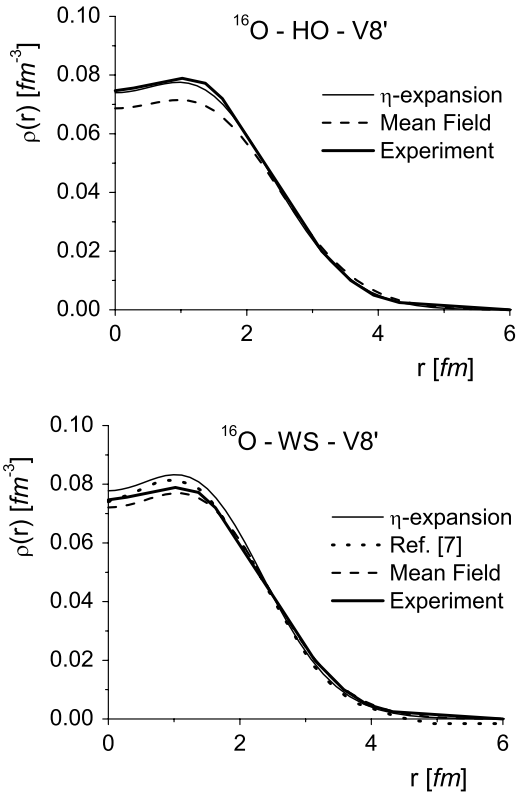

FIG. 8. The same as in Fig, 5, but with mean-field wave functions chosen so as to better reproduce the experimental density. The value of the rms radius is $\langle r^2\rangle^{1/2} = 2.73$ fm with HO wave functions and $\langle r^2\rangle^{1/2} = 2.71$ fm with WS wave functions. The value of the HO parameter is $a = 1.81$ fm, and the parameters of the WS well are $V_0 = 53.0$ fm, $R_0 = 3.45$ MeV, and $a_0 = 0.7$ fm.

Eq. (7), we have

$$\langle \hat{V}\rangle = \sum_n \langle V^{(n)}\rangle, \tag{27}$$

with

$$\langle V^{(n)}\rangle = \int d\boldsymbol{r}_1 d\boldsymbol{r}_2\, v^{(n)}(r_{12})\rho_2^{(n)}(\boldsymbol{r}_1,\boldsymbol{r}_2), \tag{28}$$

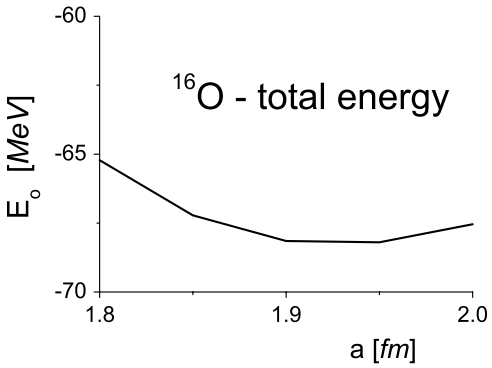

FIG. 7. The ground-state energy of ^{16}O versus the HO parameter a calculated with the η expansion and the $V8'$ interaction, by use of the correlation functions shown in Fig. 3.

where

$$\rho_2^{(n)}(\boldsymbol{r}_1,\boldsymbol{r}_2) = \langle\psi_o|\hat{\rho}_2^{(n)}|\psi_o\rangle \tag{29}$$

is the expectation value of the state-dependent TBD matrix operator

$$\hat{\rho}_2^{(n)}(\tilde{\boldsymbol{r}}_1,\tilde{\boldsymbol{r}}_2) = \sum_{i<j}\delta(\boldsymbol{r}_i-\tilde{\boldsymbol{r}}_1)\,\delta(\boldsymbol{r}_j-\tilde{\boldsymbol{r}}_2)\prod_k \delta(\tilde{\boldsymbol{r}}_k-\tilde{\boldsymbol{r}}'_k)\hat{\mathcal{O}}_{ij}^{(n)}; \tag{30}$$

with the operator $\hat{O}^{(n)}$ in Eq. (30) being the one appearing in the definition of the two-body interaction. In our calculations, with two-body interaction (7), we therefore use the following expression for the ground-state energy:

$$E_o = -\frac{\hbar^2}{2M_N}\int d\boldsymbol{r}_1[\nabla_1\cdot\nabla_{1'}\,\rho(\boldsymbol{r}_1,\boldsymbol{r}'_1)]_{\boldsymbol{r}_1=\boldsymbol{r}'_1} + \sum_n\int d\boldsymbol{r}_1 d\boldsymbol{r}_2\, v^{(n)}(r_{12})\rho_2^{(n)}(\boldsymbol{r}_1,\boldsymbol{r}_2), \tag{31}$$

which we evaluated by performing the cluster expansion of Eqs. (21) and (26) using Eqs. (16a) and (16b), with the operator $\hat{A}$ given by Eqs. (20) and (30), respectively.

The knowledge of the OBMD and TBD matrices allows one to calculate, besides the ground-state energy, other relevant

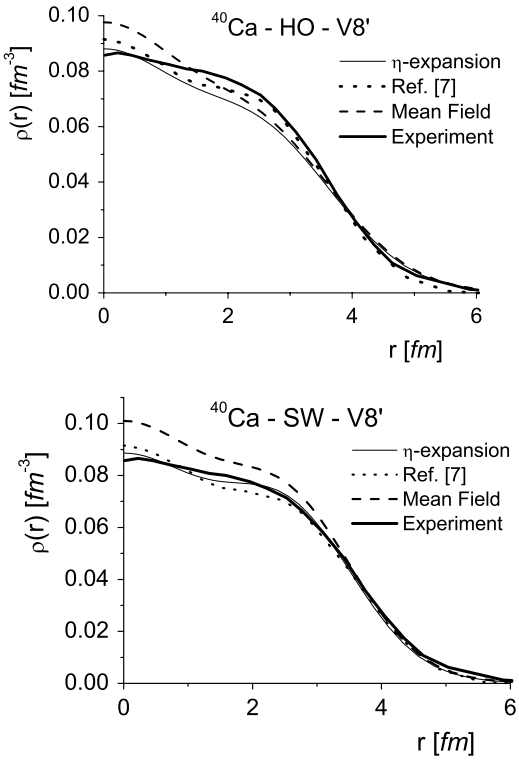

FIG. 9. The same as in Fig. 8, but for ^{40}Ca. The value of the rms radius is $\langle r^2\rangle^{1/2} = 3.56$ fm with HO wave functions and $\langle r^2\rangle^{1/2} = 3.34$ fm with WS wave functions. The value of the HO parameter is $a = 2.00$ fm, and the parameters of the WS well are $V_0 = 50.0$ MeV, $R_0 = 5.0$ fm, and $a_0 = 0.515$ fm.

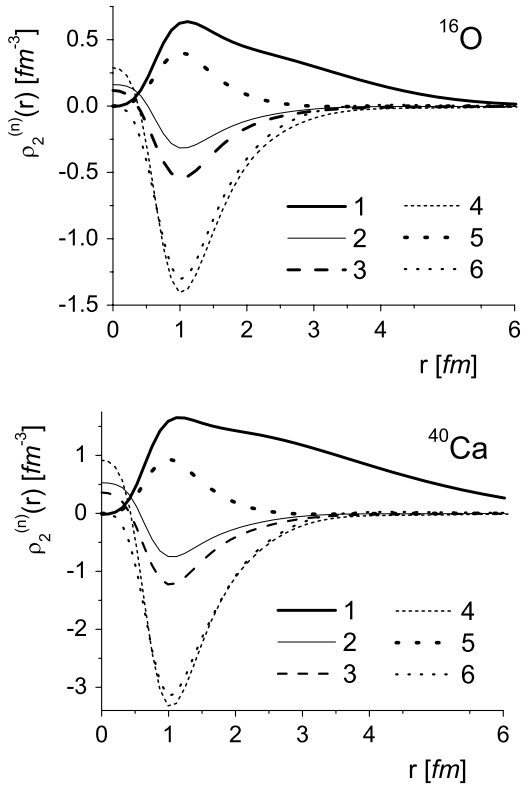

FIG. 10. The TBDs [Eq. (59)] of ^{16}O and ^{40}Ca integrated over proper coordinates [see Eq. (59)] corresponding to the correlation functions of Fig. 3 (^{16}O) and Fig. 4 (^{40}Ca).

quantities, e.g., the density distribution.

$$\rho(\boldsymbol{r}) \;=\; \rho(\boldsymbol{r}_1 = \boldsymbol{r}'_1 \equiv \boldsymbol{r}); \tag{32}$$

the mean square radius of the distribution,

$$\langle r^2\rangle \;=\; \int d\boldsymbol{r}\, r^2\, \rho(\mathbf{r}); \tag{33}$$

and, eventually, the nucleon momentum distribution,

$$n(\boldsymbol{k}) \;=\; \frac{1}{(2\pi)^3} \int d\boldsymbol{r}_1 d\boldsymbol{r}'_1\, e^{i\,\boldsymbol{k}\cdot(\boldsymbol{r}_1-\boldsymbol{r}'_1)}\, \rho(\boldsymbol{r}_1, \boldsymbol{r}'_1), \tag{34}$$

with normalization

$$\int d\boldsymbol{k} n(\boldsymbol{k}) \;=\; A. \tag{35}$$

The normalization of the OBD, OBMD, and TBD matrices are as follows:

$$\int d\boldsymbol{r}\rho(\boldsymbol{r}) \;=\; A, \tag{36}$$

$$\int d\boldsymbol{r}'_1\, \rho(\boldsymbol{r}_1, \boldsymbol{r}'_1) \;=\; \rho(\boldsymbol{r}_1), \tag{37}$$

$$\int d\boldsymbol{r}_1\, d\boldsymbol{r}_2\, \rho_2^c(\boldsymbol{r}_1, \boldsymbol{r}_2) \;=\; \frac{A(A-1)}{2}; \tag{38}$$

and the OBMD and TBD matrices satisfy the following relations:

$$\int d\boldsymbol{r}_j\, \rho(\boldsymbol{r}_i, \boldsymbol{r}_j)\, \rho(\boldsymbol{r}_j, \boldsymbol{r}_k) \;=\; \rho(\boldsymbol{r}_i, \boldsymbol{r}_k), \tag{39}$$

$$\int d\boldsymbol{r}_2\, \rho_2^c(\boldsymbol{r}_1, \boldsymbol{r}_2) = \frac{A-1}{2}\, \rho(\boldsymbol{r}_1). \tag{40}$$

It is useful at this moment to recall the form of $\rho(\boldsymbol{r}_1)$, $\rho(\boldsymbol{r}_1, \boldsymbol{r}'_1)$, and $\rho_2(\boldsymbol{r}_1, \boldsymbol{r}_2)$ predicted by the SM (or mean-field) approximation. In this case one has $\psi_o = \phi_o = (A!)^{-1/2}\det\{\varphi_{\alpha_i}(\boldsymbol{x}_j)\}$, with the single-particle orbitals given by $\varphi_\alpha(\boldsymbol{x}) = \varphi_a(\boldsymbol{r})\, \chi_\sigma^{1/2}\, \xi_\tau^{1/2}$, where $\alpha \equiv \{a;\sigma;\tau\} = \{n, l, m;\sigma;\tau\}$. For closed-shell nuclei with $N = Z$ and disregarding any Coulomb interaction, one obtains

$$\rho_{\rm SM}(\boldsymbol{r}_1) = \sum_\alpha |\varphi_\alpha(\boldsymbol{x}_1)|^2 = 4\, \rho_o(\boldsymbol{r}_1), \tag{41}$$

$$\rho_{\rm SM}(\boldsymbol{r}_1, \boldsymbol{r}'_1) = \sum_\alpha \varphi^\star_\alpha(\boldsymbol{x}_1)\varphi_\alpha(\boldsymbol{x}'_1) = 4\, \rho_o(\boldsymbol{r}_1, \boldsymbol{r}'_1), \tag{42}$$

with the sum over α running over the occupied SM states below the Fermi level, and

$$\rho_o(\boldsymbol{r}_1) = \sum_a |\varphi_a(\boldsymbol{r}_1)|^2\,, \tag{43}$$

$$\rho_o(\boldsymbol{r}_1, \boldsymbol{r}'_1) = \sum_a \varphi^\star_a(\boldsymbol{r}_1)\, \varphi_a(\boldsymbol{r}'_1). \tag{44}$$

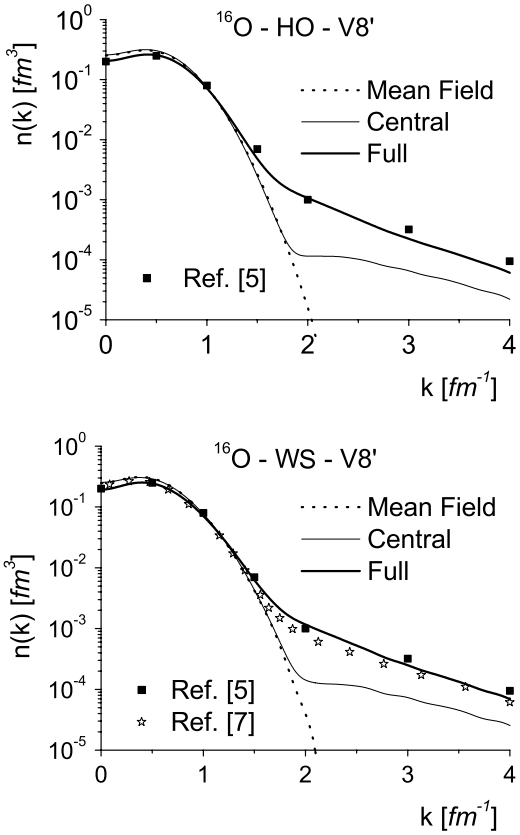

FIG. 11. The momentum distributions of ^{16}O corresponding to harmonic oscillator (top) and Woods-Saxon (bottom) wave functions, giving the best density shown in Fig. 8. The thin solid curves include only the central correlation function, whereas the thick solid curves include all of them. Our results are compared with the results of Ref. [7] (stars), obtained with the same correlation functions. The results of Ref. [5] obtained within the variational Monte Carlo approach using the $AV14$ interaction are also shown by full squares. The value of the kinetic energy obtained by integrating $n(k)$ are $\langle T\rangle = 297.87$ MeV (central, HO), $\langle T\rangle = 476.55$ MeV (full, HO); $\langle T\rangle = 306.99$ MeV (central, WS), and $\langle T\rangle = 494.48$ MeV (full, WS). In this and the following figures, the normalization of $n(k)$ is $4\pi \int n(k)k^2dk = 1$.

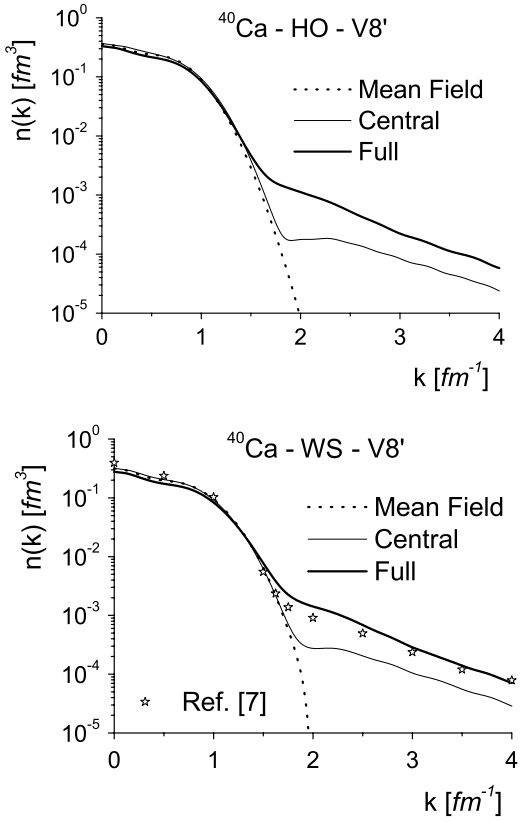

FIG. 12. The same as in Fig. 11, but for ^{40}Ca and correlation functions from Fig. 4 and mean-field wave functions giving the best charge density of Fig. 9. The value of the kinetic energy obtained by integrating $n(k)$ are $\langle T\rangle = 782.87$ MeV (central, HO), $\langle T\rangle = 1178.45$ MeV (full, HO); $\langle T\rangle = 836.24$ MeV (central, WS), and $\langle T\rangle = 1245.21$ MeV (full, WS).

For the TBD matrix one obtains

$$\rho_2^{\rm SM}(\boldsymbol{r}_1,\boldsymbol{r}_2) = \frac{1}{2}\sum_{\alpha\beta}[\,\varphi^\star_\alpha(\boldsymbol{x}_1)\,\varphi^\star_\beta(\boldsymbol{x}_2)\,\varphi_\alpha(\boldsymbol{x}_1)\,\varphi_\beta(\boldsymbol{x}_2) - \varphi^\star_\alpha(\boldsymbol{x}_1)\,\varphi^\star_\beta(\boldsymbol{x}_2)\,\varphi_\beta(\boldsymbol{x}_1)\,\varphi_\alpha(\boldsymbol{x}_2)] = \frac{1}{2}\,4\,[4\,\rho_o(\boldsymbol{r}_1)\,\rho_o(\boldsymbol{r}_2) - \rho_o(\boldsymbol{r}_1,\boldsymbol{r}_2)\,\rho_o(\boldsymbol{r}_2,\boldsymbol{r}_1)], \tag{45}$$

where $\rho_o(\boldsymbol{r}_i) = \rho_o(\boldsymbol{r}_i,\boldsymbol{r}_i)$.

When OBMD matrix (21) is evaluated with correlated wave functions (6) at first order of the η expansion, the following expression is obtained:

$$\rho(\boldsymbol{r}_1,\boldsymbol{r}'_1) = \rho_{\rm SM}(\boldsymbol{r}_1,\boldsymbol{r}'_1) + \rho_H(\boldsymbol{r}_1,\boldsymbol{r}'_1) + \rho_S(\boldsymbol{r}_1,\boldsymbol{r}'_1), \tag{46}$$

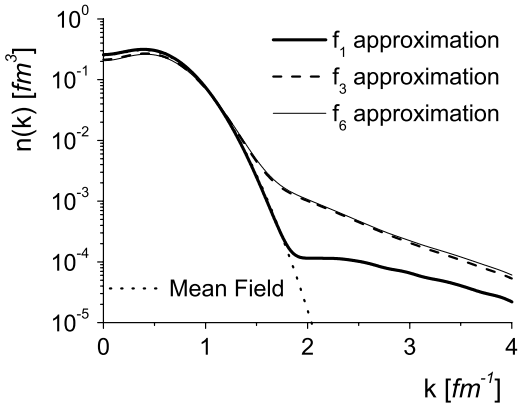

FIG. 13. The effect of the various correlation functions on the momentum distribution of ^{16}O. f_1 approximation, only central correlation; f_3 approximation, $f^{(2)} = f^{(3)} = f^{(5)} = 0$; f_6 approximation, full correlation set, $n = 1,\ldots,6$. Calculations were performed with correlation functions from Fig. 3 and HO wave functions.

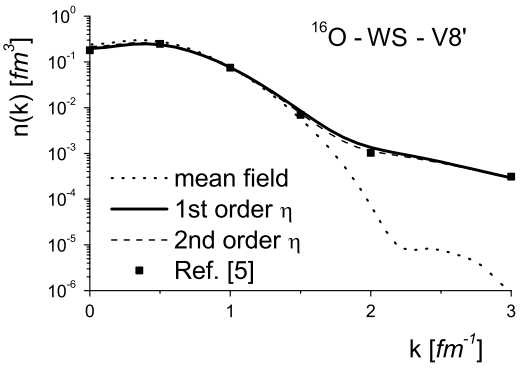

FIG. 14. The convergence of the momentum distributions of ^{16}O calculated with consideration of the first and second orders of the η expansion [see Eqs. (16a), (16b), and (16c)], Woods-Saxon mean-field wave functions, the f_3 approximation, and the correlation functions of Fig. 3. Our results are compared with the results of Ref. [5] obtained within the variational Monte Carlo approach and the $AV14$ interaction.

with

$$\rho_H(\boldsymbol{r}_1,\boldsymbol{r}_1') = \int d\boldsymbol{r}_2\,[H_D(\boldsymbol{r}_{12},\boldsymbol{r}_{1'2})\,\rho_o(\boldsymbol{r}_1,\boldsymbol{r}_1')\,\rho_o(\boldsymbol{r}_2) - H_E(\boldsymbol{r}_{12},\boldsymbol{r}_{1'2})\,\rho_o(\boldsymbol{r}_1,\boldsymbol{r}_2)\,\rho_o(\boldsymbol{r}_2,\boldsymbol{r}_1')], \quad (47a)$$

$$\rho_S(\boldsymbol{r}_1,\boldsymbol{r}_1') = -\int d\boldsymbol{r}_2 d\boldsymbol{r}_3 \rho_o(\boldsymbol{r}_1,\boldsymbol{r}_2) \times [H_D(r_{23})\rho_o(\boldsymbol{r}_2,\boldsymbol{r}_1')\rho_o(\boldsymbol{r}_3) - H_E(r_{23})\rho_o(\boldsymbol{r}_2,\boldsymbol{r}_3)\rho_o(\boldsymbol{r}_3,\boldsymbol{r}_1')]. \quad (47b)$$

Here, the subscripts H and S, whose physical meanings are explained in Sec. VII, stand for *hole* and *spectator*, respectively, and

$$H_{D(E)}(\boldsymbol{r}_{12},\boldsymbol{r}_{1'2}) = \sum_{p,q=1}^{6} f^{(p)}(r_{12})\,f^{(q)}(r_{1'2})\,C_{D(E)}^{(p,q)}(\boldsymbol{r}_{12},\boldsymbol{r}_{1'2}) - C_{D(E)}^{(1,1)}(\boldsymbol{r}_{12},\boldsymbol{r}_{1'2}), \quad (48a)$$

$$H_{D(E)}(r_{23}) = \sum_{p,q=1}^{6} f^{(p)}(r_{23})\,f^{(q)}(r_{23})\,C_{D(E)}^{(p,q)}(r_{23},r_{23}) - C_{D(E)}^{(1,1)}(r_{23},r_{23}), \quad (48b)$$

where the direct (D) and exchange (E) coefficients $C_{D(E)}^{(p,q)}(\mathbf{r}_{ij},\mathbf{r}_{kl})$ and $C_{D(E)}^{(p,q)}(r_{ij},r_{ij})$ result from the *spin* and *isospin* summation, with their dependence on the coordinates originating from the tensor operator [note that $C_{D,E}^{(p,q)}(r_{ij},r_{ij})$, unlike $C_{D,E}^{(p,q)}(\mathbf{r}_{ij},\mathbf{r}_{kl})$, is not angle dependent]; the explicit expressions of these coefficients within the f_6 and f_3 approximations are given in Appendix C.

As for the correlated TBD matrix defined by Eq. (29), it reads as follows:

$$\rho_2^{(n)}(\boldsymbol{r}_1,\boldsymbol{r}_2) = \rho_2^{\mathrm{SM}}(\boldsymbol{r}_1,\boldsymbol{r}_2) + \rho_A^{(n)}(\boldsymbol{r}_1,\boldsymbol{r}_2) + \rho_B^{(n)}(\boldsymbol{r}_1,\boldsymbol{r}_2) + \rho_C^{(n)}(\boldsymbol{r}_1,\boldsymbol{r}_2) + \rho_D^{(n)}(\boldsymbol{r}_1,\boldsymbol{r}_2), \quad (49)$$

with

$$\rho_A^{(n)}(\boldsymbol{r}_1,\boldsymbol{r}_2) = \frac{1}{A(A-1)}\Bigg\{\sum_{p,q=1}^{6} f_{12}^{(p)} f_{12}^{(q)} \sum_{r,s=1}^{6} \times \Big[K_{(p,n)}^{(r)} K_{(r,q)}^{(s)}\,A_D^{(s)}\,\rho_o(\boldsymbol{r}_1)\,\rho_o(\boldsymbol{r}_2) - K_{(p,n)}^{(r)} K_{(r,q)}^{(s)} A_E^{(s)} \rho_o(\boldsymbol{r}_1,\boldsymbol{r}_2)\rho_o(\boldsymbol{r}_2,\boldsymbol{r}_1)\Big] - \Big[A_D^{(n)}\rho_o(\boldsymbol{r}_1)\rho_o(\boldsymbol{r}_2) - A_E^{(n)}\rho_o(\boldsymbol{r}_1,\boldsymbol{r}_2)\rho_o(\boldsymbol{r}_2,\boldsymbol{r}_1)\Big]\Bigg\}, \quad (50)$$

$$\rho_B^{(n)}(\boldsymbol{r}_1,\boldsymbol{r}_2) = \frac{1}{A(A-1)} \times \int d\boldsymbol{r}_3 \sum_{\mathcal{P}} \left[\sum_{p,q=1}^{6} f_{13}^{(p)} f_{13}^{(q)} B_{(n),\mathcal{P}}^{(p,q)} - B_{(n),\mathcal{P}}^{(1,1)}\right] \times \rho_o(\boldsymbol{r}_1,\boldsymbol{r}_{\mathcal{P}\{1\}})\,\rho_o(\boldsymbol{r}_2,\boldsymbol{r}_{\mathcal{P}\{2\}})\,\rho_o(\boldsymbol{r}_3,\boldsymbol{r}_{\mathcal{P}\{3\}}), \quad (51)$$

$$\rho_C^{(n)}(\boldsymbol{r}_1,\boldsymbol{r}_2) = \frac{1}{A(A-1)} \times \int d\boldsymbol{r}_3 \sum_{\mathcal{P}} \left[\sum_{p,q=1}^{6} f_{23}^{(p)} f_{23}^{(q)} C_{(n),\mathcal{P}}^{(p,q)} - C_{(n),\mathcal{P}}^{(1,1)}\right] \times \rho_o(\boldsymbol{r}_1,\boldsymbol{r}_{\mathcal{P}\{1\}})\,\rho_o(\boldsymbol{r}_2,\boldsymbol{r}_{\mathcal{P}\{2\}})\,\rho_o(\boldsymbol{r}_3,\boldsymbol{r}_{\mathcal{P}\{3\}}), \quad (52)$$

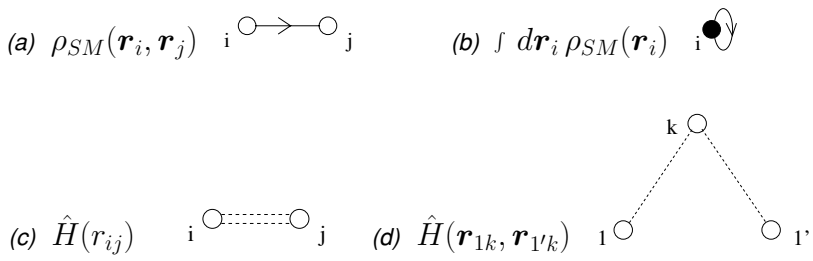

FIG. 15. Basic elements used to construct the Mayer diagrams in Figs. 16 and 17. The elements (c) and (d) are defined by Eqs. (60) and (61), respectively.

TABLE I. The results of the benchmark calculation of the ground-state energy of ^{16}O obtained by use of the $V8'$ interaction [36], the correlation functions shown in Fig. 1 [9], and harmonic-oscillator-mean field wave functions with parameter $a = 2$ fm (see Appendix A). The results of the η expansion obtained in this paper are compared with the FHNC/SOC results of Ref. [9]. $\langle \hat{V} \rangle$ is the average potential energy, $\langle \hat{T} \rangle$ the average kinetic energy, $E \equiv E_o = \langle \hat{V} \rangle + \langle \hat{T} \rangle$ the total energy, and E/A the total energy per particle. The kinetic energy of the center-of-mass motion has been subtracted from the expectation value of the kinetic-energy operator. All quantities are in mega-electron-volt.

Approach	$\langle \hat{V} \rangle$	$\langle \hat{T} \rangle$	E	E/A
η expansion, this paper	−390.37	323.50	−65.90	−4.12
FHNC/SOC, Ref. [9]	−390.30	325.18	−65.12	−4.07

$$\rho_D^{(n)}(\boldsymbol{r}_1, \boldsymbol{r}_2) = \frac{1}{A(A-1)} \frac{1}{2} \int d\boldsymbol{r}_3 d\boldsymbol{r}_4 \sum_{\mathcal{P}} \left[\sum_{p,q=1}^{6} f_{34}^{(p)} f_{34}^{(q)} \times \sum_{r=1}^{6} K_{(p,q)}^{(r)} D_{(n),\mathcal{P}}^{(r)} - D_{(n),\mathcal{P}}^{(1)} \right] \rho_o(\boldsymbol{r}_1, \boldsymbol{r}_{\mathcal{P}\{1\}}) \times \rho_o(\boldsymbol{r}_2, \boldsymbol{r}_{\mathcal{P}\{2\}})\, \rho_o(\boldsymbol{r}_3, \boldsymbol{r}_{\mathcal{P}\{3\}})\, \rho_o(\boldsymbol{r}_4, \boldsymbol{r}_{\mathcal{P}\{4\}}). \tag{53}$$

Equations (50)–(53) deserve a few explanations; $A_{D(E)}^{(n)}$, $B_{(n),\mathcal{P}}^{(p,q)}$, $C_{(n),\mathcal{P}}^{(p,q)}$, and $D_{(n),\mathcal{P}}^{(r)}$ are the result of the spin-isospin summations and they are, in general, function of the coordinates (see Appendix C); the remaining summations over the spatial quantum numbers are then expressed in terms of combinations of OBMD matrices; the subindex $\mathcal{P}$ in these factors stands for all possible permutations of the states but the *unlinked* one and the subindex $\mathcal{P}\{i\}$ stands for the corresponding index resulting from the particular permutations; finally, the matrices $K_{(p,q)}^{(r)}$ are proper *numerical* combinations of the spin-isospin operators $\hat{\mathcal{O}}_{ij}^{(n)}$ and are defined by the following relation:

$$\hat{\mathcal{O}}_{ij}^{(p)} \hat{\mathcal{O}}_{ij}^{(q)} = \sum_{r=1}^{6} K_{(p,q)}^{(r)} \hat{\mathcal{O}}_{ij}^{(r)}. \tag{54}$$

Note that even if we are dealing with two-body correlations and interactions we end up with three- and four-body operators, because, e.g., terms like $\hat{\mathcal{O}}_{12}^{(p)} \hat{\mathcal{O}}_{13}^{(q)}$, for any p, q, cannot be further reduced. Thus the first-order η expansion for the energy gets contributions from up to four-body clusters. Note that Eqs. (47a) and (47b) for the OBMD matrix were already obtained previously, e.g., in Ref. [35], whereas Eqs. (50)–(53), to our knowledge, are given for the first time in this paper.

From the definition of the nucleon momentum distribution, Eq. (34), we can obtain the expectation value of the kinetic-energy operator as

$$\langle \hat{T} \rangle = \frac{\hbar^2}{2\,M_N} \int d\boldsymbol{k}\, k^2\, n(\boldsymbol{k}), \tag{55}$$

and Eq. (31) finally becomes

$$E_o = \frac{\hbar^2}{2\,M_N} \int d\boldsymbol{k}\, k^2\, n(\boldsymbol{k}) + \sum_n \int d\boldsymbol{r}_1 d\boldsymbol{r}_2\, v^{(n)}(r_{12}) \times \rho_2^{(n)}(\boldsymbol{r}_1, \boldsymbol{r}_2), \tag{56}$$

with $\rho_2^{(n)}(\boldsymbol{r}_1, \boldsymbol{r}_2)$ given by Eq. (49). This is the final expression that has been used to calculate the ground-state energy by the following procedure: We calculate at the same order both $n(k)$ and $\rho_2^{(n)}(\boldsymbol{r}_1, \boldsymbol{r}_2)$; then, by placing them in Eq. (56) and performing the summation over n, we obtain the ground-state energy E_0. Calculations are performed with a given, fixed form for the correlation functions and considering as variational parameters the parameters of the mean-field wave functions. To begin, in the next subsection the results of a benchmark calculation aimed at investigating the convergence of the expansion are presented.

B. A benchmark calculation for ^{16}O and ^{40}Ca: Comparison between the η expansion and the fermion-hypernetted-chain–single-operator chain approach with truncated $V8'$ and $U14$ interactions

To investigate the convergence of the η expansion, we performed a benchmark calculation consisting of a comparison of Eq. (56) with the energy predicted by the FHNC–single-operator-chain (SOC) approach. Namely, we calculated the ground-state properties of ^{16}O and ^{40}Ca by using the first six components of the $V8'$ [36] and $U14$ [37] interactions, respectively (these model interactions are usually referred to as the *truncated* $V8'$ and $U14$ interactions). The results we obtained are compared with the results we obtained with FHNC/SOC by using the same interaction, the same mean-field wave functions, and the same correlation functions. The six correlation functions used in the calculation for ^{16}O, corresponding to the $V8'$ interaction, are shown in Fig. 1, and the results of the energy calculation are presented in Tables I and II. It can be seen that the cluster expansion results are very similar to the ones provided by the FHNC/SOC method; particularly worth mentioning is the almost identical value of the mean kinetic energy, which means that the nucleon

TABLE II. The contributions [see Eq. (27)] $\langle V^{(n)} \rangle$ of the first six channels of the $V8'$ interaction to the average potential energy $\langle \hat{V} \rangle$ shown in Table I. All quantities are in mega-electron-volts.

Approach	$\langle V^c \rangle$	$\langle V^\sigma \rangle$	$\langle V^\tau \rangle$	$\langle V^{\sigma\tau} \rangle$	$\langle V^t \rangle$	$\langle V^{t\tau} \rangle$	$\langle \hat{V} \rangle = \sum_n \langle V^{(n)} \rangle$
η expansion, this paper	0.6	−35.4	−10.1	−172.8	−0.03	−172.7	−390.37
FHNC/SOC, Ref. [9]	0.7	−40.1	−10.6	−180.0	0.07	−160.3	−390.30

TABLE III. The results of the benchmark calculation of the ground-state energy of ^{40}Ca obtained by use of the six-component truncated Urbana $U14$ interaction, the correlation functions shown in Fig. 2 [8], and harmonic-oscillator-mean field wave functions with parameter $a = 1.654$ fm [see Eq. (A2)]. The results of the η expansion obtained in this paper are compared with the FHNC/SOC results of Ref. [8]. Notations are the same as in Table I. All quantities are in mega-electron-volts.

Approach	$\langle\hat{V}\rangle$	$\langle\hat{T}\rangle$	E	E/A
η expansion, this paper	−1655.15	1425.90	−229.25	−5.73
FHNC/SOC, Ref. [8]	−1891.20	1576.40	−314.80	−7.87

momentum distributions predicted by the two methods are very similar. The results of the calculation for ^{40}Ca, corresponding to the truncated $U14$ interaction [37] and to the mean field and correlation functions shown in Fig. 2, are presented in Tables III and IV, where they are compared with the results of the FHNC/SOC approach of Ref. [8]. Because the mean-field wave functions and correlation functions are the same in the two calculations, any difference between our results and those of Ref. [8] has to be ascribed, as in the case of ^{16}O, to the contributions that are left out in the cluster expansion. It can be seen that the difference between the two approaches is larger in ^{40}Ca than in the ^{16}O case, the largest difference arising from the spin-isospin interaction, which as a matter of fact is of a longer range in ^{40}Ca (see Fig. 2).

To sum up, it seems that the convergence of the η expansion for the ground-state energy is a satisfactory one.

V. APPLICATION OF THE η EXPANSION TO THE NUCLEI ^{16}O AND ^{40}Ca: THE GROUND-STATE ENERGY, RADIUS, AND DENSITIES WITH THE FULL $V8'$ INTERACTION

In Ref. [7], by use of the full $V8'$ interaction that includes the spin-orbit contributions $v^{(7)}$ and $v^{(8)}$, several ground-state properties of ^{16}O and ^{40}Ca were calculated within the FHNC/SOC approach, namely the ground-state energy, the density, and the momentum distributions. For this reason, we have also calculated the ground-state properties of ^{16}O and ^{40}Ca by using the η expansion and the correlation functions of Ref. [7], which are shown in Figs. 3 and 4, respectively. The FHNC/SOC calculation of Ref. [7] was performed within the f_6 approximation. We have also used such an approximation but, unlike in Ref. [7], here we have disregarded the $v^{(7)}$ and $v^{(8)}$ components of the $V8'$ interaction. For such a reason, a direct comparison of the results for the potential energy is not possible, whereas a comparison of the average kinetic energy is fully meaningful. The results of the comparison are presented in Tables V and VI for ^{16}O, and in Tables VII and VIII for ^{40}Ca. The differences between the η expansion and the FHNC results should probably be ascribed to both the long tail of the tensor-isospin correlation function $f^{t\tau}$, which, in principle, could affect the convergence of the cluster expansion, and to the contribution of the $v^{(7)}$ and $v^{(8)}$ components disregarded in the η-expansion calculation. As far as the latter is concerned, we have estimated the effect of the inclusion of the angular-momentum-dependent terms by using the nuclear-matter results of Ref. [7], finding indeed a better agreement with the FHNC approach.

The results we have obtained deserve the following comments:

(i) We have compared our results obtained with the truncated $V8'$ interaction and the f_6 approximation but using the full $V8'$ potential that includes the $v^{(7)}$ and $v^{(8)}$ components. Because in both calculations the same mean-field wave function and correlation functions have been used, the differences between the two results have to be ascribed to the terms left out in the cluster expansion. Our estimate of the contribution of $v^{(7)}$ and $v^{(8)}$, based on nuclear-matter results, shows that this seems indeed to be the case.

(ii) The average kinetic energy obtained in [7] agrees with the one obtained by our approach; we will indeed show that the momentum distribution, from which the kinetic energy is obtained [see Eq. (55)], is in very good agreement with the one obtained in [7]. Some discrepancies are still present as far as the potential energy is concerned, but obtaining a full agreement between the lowest-order cluster expansion and the FHNC/SOC approaches would be beyond reasonable expectations.

(iii) The overall value of the ground-state energy obtained in this section is reasonably closer to the experimental one ($\simeq$8 MeV nucleon), and it appears that the η expansion provides a reasonable wave function as far as the expectation value of the Hamiltonian is concerned.

By letting $\boldsymbol{r}_1 = \boldsymbol{r}'_1 \equiv \boldsymbol{r}$ in Eq. (46), we obtain the matter density at first order of the η expansion in the following form

$$\rho(\boldsymbol{r}) = \rho_{\rm SM}(\boldsymbol{r}) + \rho_H(\boldsymbol{r}) + \rho_S(\boldsymbol{r}), \tag{57}$$

with

$$\rho_H(\boldsymbol{r}) = \int d\boldsymbol{r}_2 \,[H_D(r_{12})\,\rho_o(\boldsymbol{r})\,\rho_o(\boldsymbol{r}_2) - H_E(r_{12})\,\rho_o(\boldsymbol{r},\boldsymbol{r}_2)\,\rho_o(\boldsymbol{r}_2,\boldsymbol{r})], \tag{58a}$$

$$\rho_S(\boldsymbol{r}) = -\int d\boldsymbol{r}_2 d\boldsymbol{r}_3 \rho_o(\boldsymbol{r},\boldsymbol{r}_2)[H_D(r_{23})\rho_o(\boldsymbol{r}_2,\boldsymbol{r})\rho_o(\boldsymbol{r}_3) - H_E(r_{23})\rho_o(\boldsymbol{r}_2,\boldsymbol{r}_3)\rho_o(\boldsymbol{r}_3,\boldsymbol{r})], \tag{58b}$$

TABLE IV. The contributions of the first six channels of the $U14$ interaction to the average potential energy $\langle\hat{V}\rangle$ shown in Table. III. Notations are the same as in Table I. All quantities are in mega-electron-volts.

Approach	$\langle V^c\rangle$	$\langle V^\sigma\rangle$	$\langle V^\tau\rangle$	$\langle V^{\sigma\tau}\rangle$	$\langle V^t\rangle$	$\langle V^{t\tau}\rangle$	$\langle\hat{V}\rangle = \sum_n \langle V^{(n)}\rangle$
η expansion, this paper	−14.57	83.20	91.93	−1353.45	11.61	−473.87	−1655.15
FHNC/SOC, Ref. [8]	−8.40	92.00	108.40	−1549.20	11.60	−565.60	−1891.20

TABLE V. The results of the calculation of the ground-state energy and radius of ^{16}O obtained by use of the full $V8'$ interaction, the correlation functions shown in Fig. 3 [7], and harmonic-oscillator (HO) mean-field wave functions. The value of the HO parameter is $a = 2.0$ fm. The results of the η expansion obtained in this paper are compared with the FHNC/SOC results of Ref. [7]. Notations are the same as in Table I. $< r^2 >^{1/2}$ is the rms radius. Energies are in mega-electron-volts, radii in femtometers.

Mean field	Approach	$\langle \hat{V} \rangle$	$\langle \hat{T} \rangle$	E	E/A	$\langle r^2 \rangle^{1/2}$
HO	η expansion, this paper	−420.39	350.39	−67.54	−4.40	2.99
HO	FHNC/SOC, Ref. [7]	−439.84	353.44	−86.40	−5.40	3.03

where $\boldsymbol{r}_{12} \equiv \boldsymbol{r} - \boldsymbol{r}_2$. We obtain the charge density by convoluting $\rho(\boldsymbol{r})$ with the charge density of the proton and by correcting for the center-of-mass motion (see, e.g. [39]). Using the mean-field wave function and the correlation functions obtained from the ground-state energy calculation with the full $V8'$ interaction (see Figs. 3 and 4 and Tables V–VIII), the densities shown in Figs. 5 and 6 for ^{16}O and for ^{40}Ca, respectively, are obtained. The results presented in Figs. 5 and 6 clearly show that the charge density calculated within the first order η expansion agrees very well with the results obtained in [7] within the FHNC/SOC approach, which indicates a very good convergence of the η expansion as far as the density is concerned.

It should however be pointed out that, as first found in [7], the density calculated with mean-field wave function that minimizes the ground-state energy strongly disagrees with the experimental density. To cure such a problem, following Ref. [7], we recalculated the density, varying the mean-field parameters to obtain an agreement with the experimental density. We take advantage of the fact that, as shown in Fig. 7, the energy minimum calculated within the η expansion is a rather shallow one. The results are shown in Figs. 8 and 9, and the comparison with the results of Ref. [7] demonstrate once again the good convergence of the η expansion.

The six different TBD distributions [Eqs.(49)–(53)] corresponding to the first six correlation operators are shown in Fig. 10 for ^{16}O (top) and ^{40}Ca (bottom): Each of these densities couples with the corresponding component of the realistic potential to give the potential energy expectation value (28). Note that the quantities shown in Fig. 10 represent integrated over the center-of-mass variable and the angular part of the relative coordinate, i.e.,

$$\rho_2^{(n)}(r) = \int \rho_2^{(n)}\Big[\boldsymbol{R} = \frac{1}{2}(\boldsymbol{r}_1 + \boldsymbol{r}_2), \quad r \equiv |\boldsymbol{r}| = |\boldsymbol{r}_1 - \boldsymbol{r}_2|\Big] d\boldsymbol{R}\, d\Omega_{\hat{\mathbf{r}}}. \tag{59}$$

VI. APPLICATION OF THE η EXPANSION TO THE NUCLEI ^{16}O AND ^{40}Ca: THE NUCLEON MOMENTUM DISTRIBUTIONS

Using the correlation functions shown in Figs. 3 and 4 and the mean-field wave functions corresponding to the best densities shown in Figs. 8 and 9, we calculated momentum distributions (34) with the OBMD matrix $\rho(\boldsymbol{r}_1, \boldsymbol{r}_1')$ given by Eq. (46). The results, obtained at first order in η (the convergence will be discussed later on), are presented in Figs. 11–14. In Figs. 11 and 12, our results are compared with the the results obtained in Ref. [7], for which the same interaction and the same correlation functions have been used, and in the case of ^{16}O, also with the results of Ref. [5], for which the $AV14$ interaction [36] and the variational Monte Carlo (VMC) approach have been used. These comparisons show these facts:

(i) Our results agree nicely with those of Refs. [7] and [5].
(ii) Short-range central correlations do not produce enough high-momentum components, although they appreciably affect the momentum distributions at $k \geqslant 2$ fm^{-1}; the inclusion of the tensor operators greatly enhances the high-momentum tail of the distribution in the region $k > 2$ fm^{-1}.
(iii) The largest effect from noncentral correlations comes from the tensor-isospin, $\hat{S}_{ij}(\boldsymbol{\tau}_i \cdot \boldsymbol{\tau}_j)$, component, particularly from its angular dependence (see Appendix C); the other components play a minor role. Thus, as shown in Fig. 13, the f_3 approximation appears to be a rather good approximation for the calculation of the momentum distributions.
(iv) The satisfactory agreement of our results with those of Refs. [7] and [5] shows that the convergence of the η expansion for $\rho(\boldsymbol{r}, \boldsymbol{r}')$ is a very good one. As a matter of fact, we have explicitly evaluated the next-order cluster contribution for ^{16}O; the results, reported in Fig. 14 with

TABLE VI. The same as in Table V but for Woods-Saxon (WS) mean-field wave functions. The parameters of the WS well are as follows: $V_0 = 42.0$ MeV, $R_0 = 3.6$ fm and $a_o = 0.55$ fm.

Mean field	Approach	$\langle \hat{V} \rangle$	$\langle \hat{T} \rangle$	E	E/A	$\langle r^2 \rangle^{1/2}$
WS	η expansion, this paper	−500.59	444.10	−56.50	−3.50	2.64
WS	FHNC/SOC, Ref. [7]	−519.68	428.16	91.52	−5.72	2.83

TABLE VII. The same as in Table V, but for ^{40}Ca; the value of the HO parameter is $a = 2.1$ fm.

Mean field	Approach	$\langle \hat{V} \rangle$	$\langle \hat{T} \rangle$	E	E/A	$\langle r^2 \rangle^{1/2}$
HO	η expansion, this paper	−1320.22	1048.22	−272.00	−6.80	3.72
HO	FHNC/SOC, Ref. [7]	−1521.20	1193.60	−327.60	−8.19	3.65

the f_3 approximation used for the correlation functions, exhibit a very good convergence.

We stress that the good convergence of the momentum distributions is a proof of the good convergence of $\langle \hat{T} \rangle$.

VII. EFFECTS OF CORRELATIONS ON THE CHARGE DENSITY AND MOMENTUM DISTRIBUTIONS: THE DIAGRAMMATIC DESCRIPTION

Within any many-body approach based on correlated wave function (6), interaction (7), and the cluster expansion technique, the various density matrices can be described by a diagrammatic representation in terms of Mayer diagrams [40,41], which provide a meaningful definition of correlations and the extent to which they affect the given quantity. In particular, the density and the momentum distributions are associated with diagrams according to the following rules (see Fig. 15):

(i) An open circle with the index i denotes the coordinate $\boldsymbol{r}_i$;
(ii) A filled circle with index i stands for integration over $\boldsymbol{r}_i$;
(iii) An oriented line joining two circles with indices i and j denotes $\rho_{SM}(\boldsymbol{r}_i, \boldsymbol{r}_j)$;
(iv) A line beginning from and ending in a circle with index i denotes $\rho_{SM}(\boldsymbol{r}_i)$;
(v) Two dashed lines joining two circles with indices i and j denote the correlation operator:

$$\hat{H}(r_{ij}) = \sum_{p,q=1}^{6} \left[f^{(p)}(r_{ij})\, f^{(q)}(r_{ij})\, \hat{\mathcal{O}}_{ij}^{(p)}\, \hat{\mathcal{O}}_{ij}^{(q)} - 1 \right]; \tag{60}$$

(vi) Two dashed lines joining two open circles with indices i and i', to another circle, with index j, denote the correlation operator:

$$\hat{H}(\boldsymbol{r}_{1j}, \boldsymbol{r}_{1'j}) = \sum_{p,q=1}^{6} \left[f^{(p)}(r_{1j})\, f^{(q)}(r_{1'j})\, \hat{\mathcal{O}}_{1j}^{(p)}\, \hat{\mathcal{O}}_{1'j}^{(q)} - 1 \right]; \tag{61}$$

Applying these rules, one can write all topologically distinct diagrams by referring to a given density matrix and collecting all diagrams containing the same number of $\hat{H}$ operators. Let us consider the first-order diagrams referring to the OBMD matrix. These are drawn in Fig. 16 and the corresponding explicit expression, in agreement with Ref. [35], reads as follows:

$$\begin{aligned}\rho(\boldsymbol{r}_1, \boldsymbol{r}_1') = {} & \rho_{SM}(\boldsymbol{r}_1, \boldsymbol{r}_1') \\ & + \int d\boldsymbol{r}_2\, \hat{H}(\boldsymbol{r}_{12}, \boldsymbol{r}_{1'2}) \left[\rho_{SM}^{\sigma,r}(\boldsymbol{r}_1, \boldsymbol{r}_1')\, \rho_{SM}^{\sigma,r}(\boldsymbol{r}_2) \right. \\ & \left. - \rho_{SM}^{\sigma,r}(\boldsymbol{r}_1, \boldsymbol{r}_2)\, \rho_{SM}^{\sigma,r}(\boldsymbol{r}_2, \boldsymbol{r}_1') \right] - \int d\boldsymbol{r}_2 d\boldsymbol{r}_3 \\ & \times \rho_{SM}^{\sigma,r}(\boldsymbol{r}_1, \boldsymbol{r}_2) \hat{H}(r_{23}) \left[\rho_{SM}^{\sigma,r}(\boldsymbol{r}_2, \boldsymbol{r}_1') \rho_{SM}^{\sigma,r}(\boldsymbol{r}_3) \right. \\ & \left. - \rho_{SM}^{\sigma,r}(\boldsymbol{r}_2, \boldsymbol{r}_3)\, \rho_{SM}^{\sigma,r}(\boldsymbol{r}_3, \boldsymbol{r}_1') \right], \end{aligned} \tag{62}$$

where $\rho_{SM}^{\sigma,r}(\boldsymbol{r}_i, \boldsymbol{r}_j)$ represents the *SM* density summed over the radial quantum numbers only, i.e., explicity depending upon the spin and isospin functions. After summation over the spin-isospin variables is carried out in Eq. (62), Eqs. (47a) and (47b) are recovered.

By joining the lines between circles 1 and $1'$ in Fig. 16, the diagrams for the one-body (diagonal) density matrix are obtained; they are shown in Fig. 17, and the corresponding expression is as follows:

$$\begin{aligned}\rho(\boldsymbol{r}) = {} & \rho_{SM}(\boldsymbol{r}) \\ & + \int d\boldsymbol{r}_2\, \hat{H}(r_{12}) \left[\rho_{SM}^{\sigma,r}(\boldsymbol{r})\, \rho_{SM}^{\sigma,r}(\boldsymbol{r}_2) \right. \\ & \left. - \rho_{SM}^{\sigma,r}(\boldsymbol{r}, \boldsymbol{r}_2)\, \rho_{SM}^{\sigma,r}(\boldsymbol{r}_2, \boldsymbol{r}) \right] - \int d\boldsymbol{r}_2 d\boldsymbol{r}_3\, \rho_{SM}^{\sigma,r}(\boldsymbol{r}, \boldsymbol{r}_2) \\ & \times \hat{H}(r_{23}) \left[\rho_{SM}^{\sigma,r}(\boldsymbol{r}_2, \boldsymbol{r})\, \rho_{SM}^{\sigma,r}(\boldsymbol{r}_3) \right. \\ & \left. - \rho_{SM}^{\sigma,r}(\boldsymbol{r}_2, \boldsymbol{r}_3)\, \rho_{SM}^{\sigma,r}(\boldsymbol{r}_3, \boldsymbol{r}) \right], \end{aligned} \tag{63}$$

which, after spin-isospin summation, coincides with Eq. (57). By means of the Mayer diagrams, the meaning of *hole* (*H*) and *spectator* (*S*) contributions introduced in Secs. IV and V [see Eqs. (47a), (47b), and (58a), (58b)] now becomes clear: The hole contribution, represented by the diagrams of Figs. 16(b) and 17(b), describes the process in which particle 1 is correlated with particle 2, whereas the spectator contribution, represented by the diagrams of Figs. 16(c) and 17(c), describes the process in which dynamical correlations are acting between particles 2 and 3. In Figs. 18 and 19 we show

TABLE VIII. The same as in Table VII but for the Woods-Saxon (WS) well with parameters $V_0 = 50.0$ MeV, $R_o = 5.3$ fm, $a_o = 0.53$ fm.

Mean field	Approach	$\langle \hat{V} \rangle$	$\langle \hat{T} \rangle$	E	E/A	$\langle r^2 \rangle^{1/2}$
WS	η expansion, this paper	−1293.96	1018.19	−275.77	−7.00	3.75
WS	FHNC/SOC Ref. [7]	−1547.20	1215.20	−332.00	−8.3	3.66

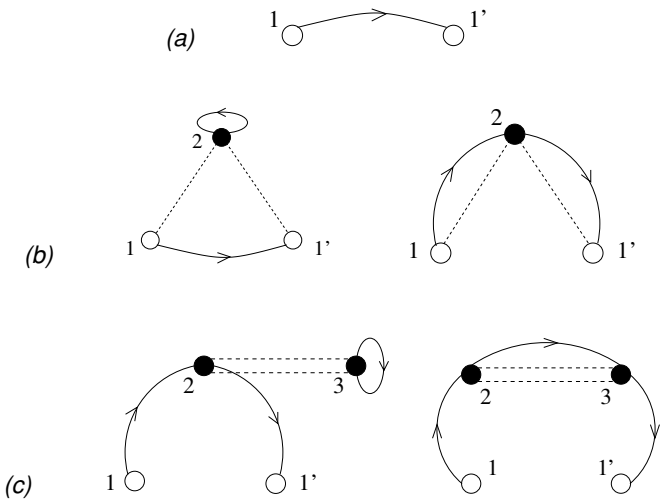

FIG. 16. Diagrammatic representation of the OBMD matrix $\rho(\boldsymbol{r}_1, \boldsymbol{r}'_1)$ in the lowest order of the η expansion [Eq. (62)]. After spin-isospin summation, (a) is the SM contribution $\rho_{SM}(\boldsymbol{r}_1, \boldsymbol{r}'_1)$ in Eq. (46) and (b) and (c) are the *hole* $\rho_H(\boldsymbol{r}_1, \boldsymbol{r}'_1)$ and *spectator* $\rho_S(\boldsymbol{r}_1, \boldsymbol{r}'_1)$ contributions, respectively, in the same equation. The direct and exchange contributions are shown on the left- and right-hand sides of the figure, respectively.

the effect of the hole and spectator contributions on the charge density and momentum distributions, respectively. It can be seen that the effect on the two quantities is very different: As far as the density is concerned, ρ_H and ρ_S are of almost the same value and of opposite sign, with a small net effect; as for the momentum distribution, the spectator contribution affects only the SM distribution by an almost constant factor of about 0.8, whereas the hole contribution creates a large amount of high-momentum components. The spectator contribution leads to a renormalization of the mean-field orbitals and to a decrease of the occupation number for states below the Fermi level, whereas the hole contribution is responsible for the

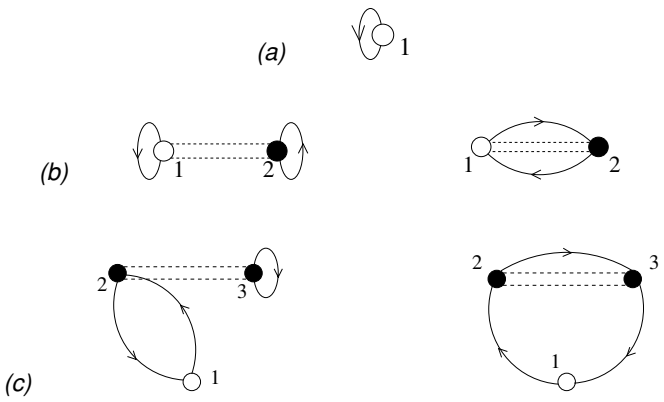

FIG. 17. The same as in Fig. 16 for the OBD matrix $\rho(\boldsymbol{r})$ of Eq. (63). After spin-isospin summation (a) is the SM contribution $\rho_{\rm SM}(\boldsymbol{r})$ in Eq. (57), and (b) and (c) are the *hole* $\rho_H(\boldsymbol{r}_1)$ and *spectator* $\rho_S(\boldsymbol{r}_1)$ contributions, respectively, in the same equation. The direct and exchange contributions are shown on the left- and right-hand sides of the figure, respectively.

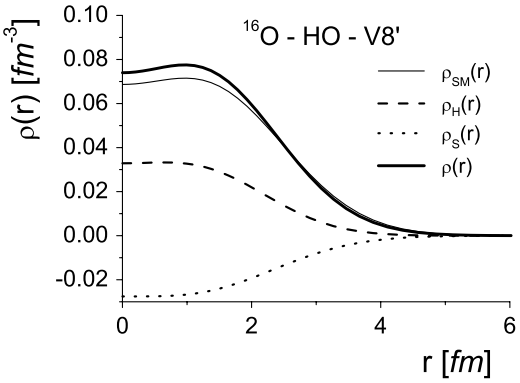

FIG. 18. The charge density of ^{16}O. Thin solid curves, SM density [Eq. (41)]; thick solid curve: correlated density [Eq. (57)] calculated with the correlation functions of Fig. 3 [7] and HO mean-field wave functions with parameter $a = 1.8$ fm; dashed curve, hole contribution [Eq. (58a)]; dotted curve, spectator contribution [Eq. (58b)].

high-momentum components. This explains and qualitatively justifies the parametrization of the momentum distribution $n(k)$ in the form $n(k) = n_o(k) + n_1(k)$, adopted in Ref. [43]. It is clear that the relative weight of hole and spectator correlations also depends on the type of mean-field wave functions; calculations show, however, that the latter, even if obtained within the most sophisticated mean-field approaches, cannot ever provide the amount of high-momentum components generated by the hole contribution, so that the high-momentum part of $n(k)$ is practically due only to hole correlations, particularly the tensor ones. Other quantities that are very sensitive to hole correlations will be discussed elsewhere [44].

So far we have discussed only the Mayer diagrams for the diagonal and nondiagonal OBD matrices. The topological structure of the TBD matrix and the relative contributions of the various associated diagrams will be discussed elsewhere.

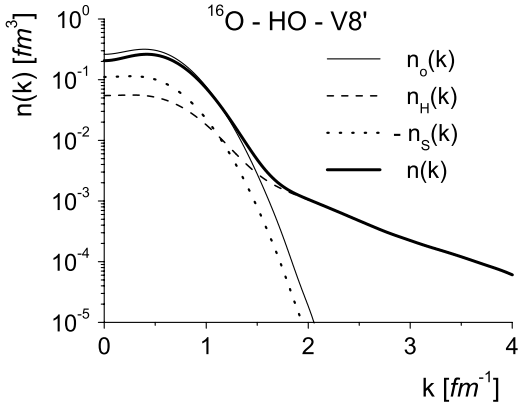

FIG. 19. The momentum distribution of ^{16}O. Thin solid curve, SM momentum distribution; thick solid curve, correlated momentum distribution (see Fig. 11); dashed curve, hole contribution; dotted curve, spectator contribution.

VIII. SUMMARY AND CONCLUSIONS

In this paper we have addressed the problem of developing a method that could be used to calculate scattering processes at medium and high energies within a realistic and parameter-free description of nuclear structure. The η expansion seems to satisfy such a requirement: As a matter of fact, it can be used within the following strategy: (i) the values of the parameters pertaining to the correlation functions and the mean-field wave functions, can be obtained from the calculation of the ground-state energy, radius and density of the nucleus, to a given order of the expansion; (ii) when these parameters are used, any scattering process can be evaluated at the same order of the cluster expansion. The method therefore appears to be a very effective, transparent, and parameter-free one. It should however be pointed out that, as with any other many-body approach, our cluster expansion approach may suffer from the well-known convergence problem, so that the role played by the disregarded higher-order terms has to be estimated. This is precisely what has been done in the present paper, with the following procedure: (i) our lowest-order results have been compared with the ones obtained within more complete approaches, e.g., the FHNC and VMC methods, and (ii) a direct calculation of the higher-order terms of the momentum distribution $n(\boldsymbol{k})$ has been performed. It turned out that the value of the ground-state energy calculated within the first-order η expansion reasonably agrees with the one obtained within the FHNC/SOC approach. The agreement is very good as far as the average kinetic energy is concerned, whereas differences occur in some of the potential-energy contributions, as should have been expected because of the complex spatial dependence of some of the components of the nucleon-nucleon interaction. Nonetheless, using the same correlation functions as in the FHNC/SOC calculation, we obtain a reasonable minimum value of the energy, with the mean-field wave function very near to the ones of the FHNC/SOC approach. Furthermore, our results for the charge density and momentum distributions show very good agreement with the results obtained within the FHNC/SOC approach and even with the VMC approach; moreover, the direct calculation of the higher-order terms in the expansion of the momentum distributions shows very good convergence of the η expansion up to very high values of the momentum.

To sum up, we have shown that, by using realistic models of the nucleon-nucleon interaction, a proper approach based on cluster expansion techniques can produce reliable approximations for those diagonal and nondiagonal density matrices that appear in various medium and high-energy scattering processes off nuclei, so that the role of nuclear effects in these processes can be reliably estimated without using free parameters to be fitted to the data. The approach has already been extended to the treatment of the FSI effects in $A(e, e'p)X$ processes at medium energies within the eikonal-Glauber multiple-scattering theory and to the calculation of nuclear and color-transparency effects. Preliminary results [22] are very encouraging. Calculations of other types of high-energy scattering processes (e.g., the total nucleon-nucleus cross section) are in progress and will be reported elsewhere [44].

ACKNOWLEDGMENTS

We are grateful to Giampaolo Co' for providing the FHNC results used in the benchmark calculation and to Adelchi Fabrocini who supplied us with the correlation functions corresponding to the full $V8'$ interaction. H.M. thanks the Department of Physics, University of Perugia, and the Istituto Nazionale di Fisica Nucleare, Sezione di Perugia, for warm hospitality and support. C. CdA expresses his gratitude to Rafael Guardiola for enlightening discussions. Support by the Italian Ministero dell'Istruzione, Università e Ricerca, through contracts COFIN03-029498 and COFIN04-025729, is gratefully acknowledged.

APPENDIX A: MEAN-FIELD WAVE FUNCTIONS

The mean-field wave functions have the general form,

$$\psi_{nlm}(\boldsymbol{r}) \;=\; R_{nl}(r)\, Y_{lm}(\theta, \varphi), \tag{A1}$$

where $R_{nl}(r)$ is the radial part and $Y_{lm}(\theta, \varphi)$ is the spherical harmonics. We have used harmonic-oscillator (HO) and Woods-Saxon (WS) wells to generate the radial part; in the HO case, we have

$$R_{nl}(r) \;=\; e^{-x/2}\, x^{l/2}\, U_{nl}\, X_{nl}^{1/2} \Psi, \tag{A2}$$

where $x = r^2/a^2$, a is the HO parameter, and

$$U_{nl} \;=\; \sum_{k=1}^{n} \frac{(-1)^k\, x^k\, n!\, 2^k\, (2l+1)!!}{(n-k)!\, k!\, (2l+2k+1)!!}, \tag{A3}$$

$$X_{nl} \;=\; \frac{2^{l-n+2}\, (2l+2n+1)!!}{(2l+1)!!^2\, n!\, \pi^{1/2}\, a^3}\,; \tag{A4}$$

whereas, in the WS case, the radial part is the solution of the radial Schrödinger equation with one-body potential of the following form

$$V_{\rm WS}(r) \;=\; -\,\frac{V_o}{1 + e^{-(r-R_o)/a_o}}. \tag{A5}$$

APPENDIX B: PARAMETRIZATION OF THE CORRELATION FUNCTIONS FOR ^{16}O AND ^{40}Ca

The correlation functions $f^{(n)}(r)$ for ^{16}O and ^{40}Ca, shown in Figs. 3 and 4, respectively, can be conveniently parametrized in the following way:

$$f^{(n)}(r) = \sum_{i=1}^{6} A_i^{(n)}\, e^{-\,B_i^{(n)}\, r^i}, \quad n = 1, \ldots, 5; \tag{B1a}$$

$$f^{(6)}(r) = A_2^{(6)} r^2 e^{-B_1^{(6)} r} \;+\; \sum_{i=2}^{6} A_i^{(6)}\, r^{i-1}\, e^{-\,B_i^{(6)}\, r^i}, \tag{B1b}$$

TABLE IX. The values of the parameters appearing in the parametrization [Eqs. (B1a) and (B1b)] of the correlation functions of ^{16}O shown in Fig. 3.

n	$A_1^{(n)}$	$A_2^{(n)}$	$A_3^{(n)}$	$A_4^{(n)}$	$A_5^{(n)}$	$A_6^{(n)}$	$B_1^{(n)}$	$B_2^{(n)}$	$B_3^{(n)}$	$B_4^{(n)}$	$B_5^{(n)}$
1	1.0005	0.37314	−1.1781	0.0	0.0	0.0	1.0	2.0	0.0	0.0	0.0
2	0.0	−0.1372	0.1916	−0.0226	−0.0141	0.0	5.0	3.5	1.0	0.13	0.0
3	0.0	−0.0795	0.1271	−0.0121	−0.0330	0.0	5.0	3.5	1.5	0.14	0.0
4	0.0	−0.3817	0.4863	−0.0535	−0.0424	0.0	4.5	3.7	1.6	0.15	0.0
5	0.0	0.0114	0.0527	−0.0702	0.0064	0.0	0.8	1.5	1.5	1.5	0.0
6	0.0	−0.1776	−0.0054	−0.0237	−0.00006	0.0	1.7	1.0	1.3	0.01	0.0

where the parameters $A_i^{(n)}$ and $B_i^{(n)}$ are given in Table IX for ^{16}O and in Table X for ^{40}Ca.

APPENDIX C: THE COEFFICIENTS OF THE ONE-BODY MIXED-DENSITY AND TWO-BODY DENSITY MATRICES RESULTING FROM THE SPIN-ISOSPIN SUMMATION

The coefficients appearing in Eqs. (48a) and (48b) for the OBMD are defined as

$$C_D^{(p,q)}(\boldsymbol{r}_{12}, \boldsymbol{r}_{1'2}) = \sum_{\sigma_1,\sigma_2,\tau_1,\tau_2} \langle \sigma_1\tau_1\,\sigma_2\tau_2 \,|\, \hat{O}_{12}^{(p)}\, \hat{O}_{1'2}^{(q)} \,|\, \sigma_1\tau_1\,\sigma_2\tau_2\rangle,$$
$$C_E^{(p,q)}(\boldsymbol{r}_{12}, \boldsymbol{r}_{1'2}) = \sum_{\sigma_1,\sigma_2,\tau_1,\tau_2} \langle \sigma_1\tau_1\,\sigma_2\tau_2 \,|\, \hat{O}_{12}^{(p)}\, \hat{O}_{1'2}^{(q)} \,|\, \sigma_2\tau_2\,\sigma_1\tau_1\rangle, \tag{C1}$$

and can be calculated analytically; their explicit values are summarized in Table XI. From this table, we can extract the expressions for $H_{D(E)}$ [Eqs. (48a) and (48b)] in the case of the f_3 approximation:

$$\begin{aligned}
H_D(r_{ij}) &= 16\left\{\left[\, f_{ij}^{(1)}\, f_{ij}^{(1)} \,-\, 1\,\right]\right. \\
&\quad \left. +9\left[f_{ij}^{(4)}\, f_{ij}^{(4)} \,+\, 2\, f_{ij}^{(6)}\, f_{ij}^{(6)}\right]\right\}, \\
H_E(r_{ij}) &= 4\left\{\left[\, f_{ij}^{(1)}\, f_{ij}^{(1)} \,-\, 1\,\right] + 9\left[f_{ij}^{(4)}\, f_{ij}^{(4)}\right.\right. \\
&\quad \left.\left. -4\, f_{ij}^{(6)}\, f_{ij}^{(6)}\,\right] + 18\left[\, f_{ij}^{(1)}\, f_{ij}^{(4)} \,+\, \right]\right\} \\
H_D(\boldsymbol{r}_{ij}, \boldsymbol{r}_{i'j}) &= 16\left(\left[\, f_{ij}^{(1)}\, f_{i'j}^{(1)} \,-\, 1\,\right] + 9\left\{f_{ij}^{(4)}\, f_{i'j}^{(4)}\right.\right. \\
&\quad \left.\left. + f_{ij}^{(6)}\, f_{i'j}^{(6)}\,[\,3\,(\hat{r}_{ij}\cdot\hat{r}_{i'j})^2 \,-\, 1\,]\right\}\right)
\end{aligned} \tag{C2}$$

$$\begin{aligned}
H_E(\boldsymbol{r}_{ij}, \boldsymbol{r}_{i'j}) &= 4\left(\left[\, f_{ij}^{(1)}\, f_{i'j}^{(1)} \,-\, 1\,\right] + 9\left\{f_{ij}^{(4)}\, f_{i'j}^{(4)}\right.\right. \\
&\quad \left. -2\, f_{ij}^{(6)}\, f_{i'j}^{(6)}\,[\,3\,(\hat{r}_{ij}\cdot\hat{r}_{i'j})^2 \,-\, 1\,]\right\} \\
&\quad \left. +9\left[\, f_{ij}^{(1)}\, f_{i'j}^{(4)} \,+\, f_{ij}^{(4)}\, f_{i'j}^{(1)}\right]\right)
\end{aligned}$$

where $\hat{r}_{ij} = \boldsymbol{r}_{ij}/|\boldsymbol{r}_{ij}|$. Using the approximation $f^{(1)} = f$ and $f^{(4)} = f^{(6)} = g$ as in Ref. [19], we obtain

$$\begin{aligned}
H_D(r_{ij}) &= 16\left[\left(f_{ij}^2 \,-\, 1\right) \,+\, 27\, g_{ij}^2\right], \\
H_E(r_{ij}) &= 4\left[\,\left(\, f_{ij}^2 \,-\, 1\right) \,-\, 27\, g_{ij}^2 \,+\, 18\, f_{ij}\, g_{ij}\,\right], \\
H_D(\boldsymbol{r}_{ij}, \boldsymbol{r}_{i'j}) &= 16\left[\,(\, f_{ij}\, f_{i'j} \,-\, 1\,) \,+\, 27\, g_{ij}\, g_{i'j}\,(\hat{r}_{ij}\cdot\hat{r}_{i'j})^2\right], \\
H_E(\boldsymbol{r}_{ij}, \boldsymbol{r}_{i'j}) &= 4\left\{(f_{ij} f_{i'j} - 1) + 27 g_{ij} g_{i'j}[1 - 2(\hat{r}_{ij}\cdot\hat{r}_{i'j})^2]\right. \\
&\quad \left. +9(f_{ij} g_{i'j} + f_{i'j} g_{ij})\right\}.
\end{aligned} \tag{C3}$$

It should be pointed out that in Refs. [19] and [35] the angular-dependent factor $(\hat{r}_{ij}\cdot\hat{r}_{i'j})^2$ has been replaced with unity. Such a replacement does not affect the nuclear transparency calculated in [19] but strongly affects the high-momentum part of the nucleon momentum distributions.

The coefficients appearing in the definition of the TBD are more involved and can be written only in terms of the spin-isospin states on which they have to be calculated:

$$\begin{aligned}
A_D^{(n=1,6)} &= \{16, 0, 0, 0, 0, 0\}, \\
A_E^{(n=1,6)} &= \{4, 12, 12, 36, 0, 0\};
\end{aligned} \tag{C4}$$

TABLE X. The same as in Table IX for the correlation functions of ^{40}Ca shown in Fig. 4.

n	$A_1^{(n)}$	$A_2^{(n)}$	$A_3^{(n)}$	$A_4^{(n)}$	$A_5^{(n)}$	$A_6^{(n)}$	$B_1^{(n)}$	$B_2^{(n)}$	$B_3^{(n)}$	$B_4^{(n)}$	$B_5^{(n)}$
1	1.00039	0.7576	−1.6015	0.0	0.0	0.0	3.9	2.9	0.0	0.0	0.0
2	0.0	−0.0573	0.0965	−0.0156	−0.0145	0.0	7.0	3.5	0.8	0.2	0.0
3	0.0	−0.0207	0.0474	−0.0019	−0.0279	0.0	8.5	3.5	2.0	0.215	0.0
4	0.0	−0.0290	0.0906	−0.0237	−0.0356	0.0	9.4	3.0	1.0	0.22	0.0
5	0.0	0.0165	0.0061	0.0009	−0.0188	0.0041	1.0	3.0	0.3	1.3	4.5
6	0.0	−0.1342	0.00013	−0.0368	0.00044	−0.00069	1.55	0.02	1.4	0.1	0.1

TABLE XI. The value of $C_D^{(p,q)}(\boldsymbol{r}_{12}, \boldsymbol{r}_{1'2})$ and $C_E^{(p,q)}(\boldsymbol{r}_{12}, \boldsymbol{r}_{1'2})$ defined in Appendix C. The order of the operator $p, q = 1, 2, \ldots, 6$ is the same as Table II. Here $\langle S_{12}S_{1'2}\rangle$ is defined as $\langle S_{12}S_{1'2}\rangle = 12[3(\hat{\boldsymbol{r}}_{12}\cdot\hat{\boldsymbol{r}}_{1'2})^2 - 1]$, with $\hat{\boldsymbol{r}} = \boldsymbol{r}/r$.

Operator p/q		1	2	3	4	5	6
1	D	16	0	0	0	0	0
	E	4	12	12	36	0	0
2	D		48	0	0	0	0
	E		−12	36	−36	0	0
3	D			48	0	0	0
	E			−12	−36	0	0
4	D				144	0	0
	E				36	0	0
5	D					$4\langle S_{12}S_{1'2}\rangle$	0
	E					$2\langle S_{12}S_{1'2}\rangle$	$6\langle S_{12}S_{1'2}\rangle$
6	D						$12\langle S_{12}S_{1'2}\rangle$
	E						$-6\langle S_{12}S_{1'2}\rangle$

$$B_{(n),\mathcal{P}}^{(p,q)}(\boldsymbol{r}_{12}, \boldsymbol{r}_{13}) = \sum_{\sigma,\tau}\langle\sigma_1\tau_1,\ \sigma_2\tau_2,\ \sigma_3\tau_3 \mid \hat{O}_{13}^{(p)}\,\hat{O}_{12}^{(n)}\,\hat{O}_{13}^{(q)} \mid \times (\sigma_1\tau_1,\ \sigma_2\tau_2,\ \sigma_3\tau_3)\rangle_{\mathcal{P}} \tag{C5}$$

$$C_{(n),\mathcal{P}}^{(p,q)}(\boldsymbol{r}_{12}, \boldsymbol{r}_{23}) = \sum_{\sigma,\tau}\langle\sigma_1\tau_1,\ \sigma_2\tau_2,\ \sigma_3\tau_3 \mid \hat{O}_{23}^{(p)}\,\hat{O}_{12}^{(n)}\,\hat{O}_{23}^{(q)} \mid \times (\sigma_1\tau_1,\ \sigma_2\tau_2,\ \sigma_3\tau_3)\rangle_{\mathcal{P}} \tag{C6}$$

$$D_{(n),\mathcal{P}}^{(q)}(\boldsymbol{r}_{12}, \boldsymbol{r}_{34}) = \sum_{\sigma,\tau}\langle\sigma_1\tau_1,\ \sigma_2\tau_2,\ \sigma_3\tau_3,\ \sigma_4\tau_4 \mid \hat{O}_{12}^{(n)}\,\hat{O}_{34}^{(q)} \mid \times (\sigma_1\tau_1,\ \sigma_2\tau_2,\ \sigma_3\tau_3,\ \sigma_4\tau_4)_{\mathcal{P}} \tag{C7}$$

where only *linked* permutations are considered; for example, in the four-body term, the identical permutation $|\,\alpha_1\beta_2\gamma_3\delta_4\rangle$ is not linked, because the only present links are between particles 12 and 34, but the two clusters are not connected; there are four unlinked permutations in this term.

[1] W. Glöckle *et al*., Phys. Rep. **274**, 107 (1996).
[2] A. Kievsky, S. Rosati, and M. Viviani, Nucl. Phys. **A551**, 241 (1993) and (private communication).
[3] H. Kamada *et al*., Phys. Rev. C **64**, 044001 (2001).
[4] S. C. Pieper, and R. B. Wiringa, Annu. Rev. Nucl. Part. Sci. **51**, 53 (2001).
[5] S. C. Pieper, R. B. Wiringa, and V. R. Pandharipande, Phys. Rev. C **46**, 1741 (1992).
[6] I. Stetcu, B. R. Barrett, P. Navratil, and J. P. Vary, Phys. Rev. C **71**, 044325 (2005).
[7] A. Fabrocini, F. Arias de Saavedra, and G. Có, Phys. Rev. C **61**, 044302 (2000) and (private communication).
[8] A. Fabrocini, F. Arias de Saavedra, G. Có, and P. Folgarait, Phys. Rev. C **57**, 1668 (1998).
[9] G. Co', and A. M. Lallena, Ann. Phys. (NY) **287**, 101 (2001).
[10] S. R. Mokhtar, M. Anguiano, G. Có, and A. M. Lallena, Ann. Phys. (NY) **293**, 67 (2001).
[11] C. Giusti and F. D. Pacati, Nucl. Phys. **A615**, 373 (1997).
[12] O. Benhar and V. R. Pandharipande, Phys. Rev. C **47**, 2218 (1993); C. Ciofi degli Atti and S. Simula, Phys. Lett. **B325**, 276 (1994).
[13] C. Ciofi degli Atti and S. Liuti, Nucl. Phys. **A532**, 235 (1991).
[14] J. Ryckebusch, S. Janssen, W. Van Nespen, and D. Debruyne, Phys. Rev. C **61**, 021603(R) (2000).
[15] C. Barbieri, C. Giusti, F. D. Pacati, and W. H. Dickhoff, Phys. Rev. C **70**, 014606 (2004).
[16] See, e.g., L. L. Frankfurt, G. A. Miller, and M. Strikman, Annu. Rev. Nucl. Part. Sci. **45**, 501 (1994); N. N. Nikolaev, Surv. High Energy Phys. **7**, 1 (1994).
[17] S. J. Brodsky and A. H. Mueller, Phys. Lett. **B206**, 685 (1988).
[18] See, e.g., B. Z. Kopeliovich, J. Nemchik, E. Predazzi, and A. Hayashigaki, Nucl. Phys. **A740**, 211 (2004).
[19] C. Ciofi degli Atti and D. Treleani, Phys. Rev. C **60**, 024602 (1999).
[20] G. Co' (private communication).
[21] M. Alvioli, Ph.D. thesis, University of Perugia, 2004.
[22] M. Alvioli, C. Ciofi degli Atti, and H. Morita, invited paper to the Second International Conference on Nuclear and Particle Physics with CEBAF at JLab, Dubrovnik, Croatia, 2003 Fiz. B **13**, 585 (2004).
[23] H. Primakoff and T. Holstein, Phys. Rev. **55**, 1218 (1939).
[24] C. Ciofi degli Atti, in *Hadronic Physics with Multi-Gev Electrons*, Les Houches Series, Nova Science Publ., New York, 1991.
[25] J. W. Clark, Prog. Part. Nucl. Phys. **2**, 89 (1979).
[26] S. C. Pieper and R. B. Wiringa, Annu. Rev. Nucl. Part. Sci. **51**, 53 (2001).
[27] R. Guardiola, Nucl. Phys. **A328**, 490 (1979).
[28] R. Guardiola and M. Portesi, J. Phys. G. **24**, L37 (1998).
[29] M. Gaudin, J. Gillespie, and G. Ripka, Nucl. Phys. **A176**, 237 (1971).
[30] O. Bohigas and S. Stringari, Phys. Lett. **B95**, 9 (1980).
[31] M. Dal Rí and S. Stringari, Nucl. Phys. **A376**, 81 (1982).
[32] O. Benhar, C. Ciofi degli Atti, S. Liuti, and G. Salmè, Phys. Lett. **B177**, 135 (1986).
[33] O. Benhar and V. R. Pandharipande, Rev. Mod. Phys. **65**, 817 (1993).
[34] S. S. Dimitrova, D. N. Kadrev, A. N. Antonov, and M. V. Stoitsov, Eur. Phys. J. A **7**, 335 (2000).
[35] F. Arias de Saavedra, G. Có, and M. M. Renis, Phys. Rev. C **55**, 673 (1997).
[36] R. B. Wiringa, V. G. J. Stoks, and R. Schiavilla, Phys. Rev. C **51**, 38 (1995).
[37] R. B. Wiringa, Phys. Rev. C **43**, 1585 (1991).
[38] I. E. Lagaris and V. Pandharipande, Nucl. Phys. **A359**, 331 (1981); **A359**, 349 (1981).
[39] L. R. B. Elton, *Nuclear Size* (Oxford University Press, London, 1961).
[40] J. E. Mayer and M. G. Mayer, *Statistical Mechanics* (Wiley, New York and London, 1940).
[41] J.-P. Blaizot and G. Ripka, *Quantum Theory of Finite Systems* (MIT Press, Cambridge, MA, 1986).
[42] H. De Vries, C. W. De Jager, and C. De Vries, At. Data Nucl. Data Tables **36**, 495 (1987).
[43] C. Ciofi degli Atti and S. Simula, Phys. Rev. C **53**, 1689 (1996).
[44] M. Alvioli, C. Ciofi degli Atti, I. Marchino, and H. Morita, nucl-th/0510079.